The Role of Diabatic Heating, Torques and Stabilities in Forcing the Radial–Vertical Circulation within Cyclones Part II: Case Study of Extratropical and Tropical Cyclones①

Zhuojian Yuan (袁卓建) and *Donald R. Johnson*
Space Science and Engineering Center, University of Wisconsin–Madison, Madison, WI 53706
Received August 11, 1997

ABSTRACT

Utilizing Eliassen's concepts, the forcing of the isentropic azimuthally–averaged mass–weighted radial–vertical circulation by diabatic heating and torques within an extratropical cyclone and a typhoon was studied through numerical simulations based on the linear diagnostic equation derived previously. The structure of the forcing associated with diabatic heating and torques was determined from quasi–Lagrangian diagnostic analyses of actual case studies. The two cyclones studied were the Ohio extratropical cyclone of 25–27 January 1978 and typhoon Nancy of 18–23 September 1979. The Ohio cyclone, which formed over the Gulf Coast and moved through Ohio and eastern Michigan, was one of the most intense storms with blizzard conditions to ever occur in this region. Typhoon Nancy which occurred over the South China Sea during the FGGE year was selected since relatively high quality assimilated data were available. Within the Ohio cyclone, the dominant internal processes forcing the mean circulation with embedded relatively strong hydrodynamic stability were the pressure torque associated with baroclinic (asymmetric) structure and the horizontal eddy angular momentum transport associated with the typical S–shaped thermal and wind structures of self–development. Within typhoon Nancy, the dominant internal process forcing the mean circulation with embedded weak hydrodynamic stability was the latent heat release.

This analysis shows that the simulated azimuthally–averaged mass–weighted radial motions within these two cyclones agree quite well with the "observed" azimuthally–averaged mass–weighted radial motions. This isentropic numerical study also provides insight into the relatively important internal forcing processes and the trade off between forcing and stability within both extratropical and tropical cyclones.

Key words: The forcing of Radial–Vertical Circulations, the stimulation of radial motion

I. INTRODUCTION

In an earlier study (Johnson and Yuan, 1998a), the perspectives of forcing the meridional circulation within a circumpolar vortex (Eliassen, 1951) and forcing the zonally–averaged isentropic meridional circulation within the circumpolar vortex (Gallimore and Johnson, 1981) were extended to determine the forcing of the azimuthally–averaged mass–weighted radial–vertical circulation within translating extratropical and tropical cyclones by torque and diabatic heating. The diagnostic equation derived in quasi–Lagrangian isentropic coordinates (Johnson and Yuan, 1998a) isolates several physical processes. These processes include the effects of 1) pressure torque (baroclinity), 2) eddy angular momentum

①This research was sponsored by NASA Grant NAG 5–81.

transport, 3) diabatic heating, 4) frictional torque, 5) inertial torque and 6) tilting of angular momentum towards or away from the local vertical axis due to cyclone's movement over the spherical earth. Since the equation is linear and diagnostic, this numerical diagnostic study does not resolve the evolution of radial motion in terms of nonlinearity and feedback between the various processes.

One purpose of this study is to link the distinct physical processes responsible for forcing the radial–vertical circulation to the development, maintenance and decay of cyclones through the use of the diagnostic equation. Another is to compare the dominant internal processes within extratropical and tropical cyclones through numerical simulation. This study also reviews the relevance of the isentropic radial–vertical circulation with its systematic transport of angular momentum and enthalpy in maintaining a balanced vortex. The numerics of the diagnostic equation for the radial–vertical circulation within cyclones are provided in Section 2, while boundary conditions are discussed in Section 3. Section 4 presents the numerical solutions and analyses of the forcing of the radial–vertical circulation for the two cyclones selected for this study, the Ohio cyclone of 25–27 January 1978 and typhoon Nancy of 18–23 September 1979. The Ohio cyclone, which formed over the Gulf Coast and moved through Ohio and Michigan, was one of the most intense storms with blizzard conditions to ever occur in this region. Typhoon Nancy, which occurred over the South China Sea during the FGGE year, was selected since relatively high quality assimilated data were available. The results are summarized in Section 5.

II. THE DIAGNOSTIC EQUATION FOR THE MEAN RADIAL–VERTICAL CIRCULATION OF CYCLONES

Since isentropic coordinates are used in the present study, all the horizontal and time derivations are performed on isentropic surfaces, which implies that $\partial()/\partial t$, $\partial()/\partial\beta$ and $\partial()/\partial\alpha$ in the following equations represent $\hat{c}()/\hat{c}t_\theta$, $\hat{c}()/\hat{c}\beta_\theta$ and $\hat{c}()/\hat{c}\alpha_\theta$ respectively. The diagnostic equation for the stream function of the azimuthally–averaged mass–weighted radial–vertical circulation in this study is a linear second order differential equation (Yuan, 1994; Johnson and Yuan, 1998a)

$$\begin{aligned}
&\frac{\hat{c}}{\hat{c}\Phi}\left(A\frac{\partial S}{\partial\Phi}+B\frac{\partial S}{\partial\bar{p}}\right)+\frac{\hat{c}}{\hat{c}\bar{p}}\left(B\frac{\partial S}{\partial\Phi}+C\frac{\partial S}{\partial\bar{p}}\right)\\
&=\frac{\hat{c}}{\hat{c}\Phi}(\alpha,\dot{\theta})+\frac{\hat{c}}{\hat{c}\bar{p}}\{-\frac{\delta}{\delta t_\theta}\overline{[(\rho J_\theta)'\frac{1}{a}(\frac{\partial\psi'}{\partial\beta})]}/\overline{(\rho J_\theta)}\}\\
&-\dot{\theta}\frac{\partial}{\partial\theta}\overline{[(\rho J_\theta)'\frac{1}{a}(\frac{\partial\psi'}{\partial\beta})]}/(\rho J_\theta)]+2\hat{g}_{az}\hat{F}/(a\sin\beta)^3\},
\end{aligned}\tag{1}$$

where ρJ_θ equal to $-(1/g)\partial p/\partial\theta$ is hydrostatic mass in an isentropic volume. Φ and $\bar{p}$ are the transformed radial and vertical coordinates respectively. They are defined by the partial differential relations [see (22) – (25) in Johnson and Yuan, 1998a] between the mass coordinates $\bar{p}(\beta,\theta,t)=g\overline{m}=g\int_\theta^{\theta_T}\overline{\rho J_\theta}\,d\theta$ and isentropic coordinates $\theta[\Phi(\beta),\bar{p}(\beta,\theta,t),t]$ (Gallimore and Johnson, 1981). For the rest of the symbols, see Appendix C. The relationships between the streamfunction S and the azimuthally–averaged mass–weighted radial and vertical motions are expressed by

$$\sin\beta(\hat{u}-\hat{w})_\beta=\frac{\partial S}{\partial\bar{p}},\tag{2}$$

$$\sin\beta\hat{\omega}_p = -\frac{\partial S}{\partial \Phi}. \tag{3}$$

In (1), coefficient A (Appendix B) relates with static stability, B with baroclinity, and C with inertial stability (Johnson and Yuan, 1998a). The terms on the right hand side of (1) represent various forcing processes. The first term represents the diabatic forcing associated with latent heat release, evaporation, radiation and heat fluxes. The second and third terms represent the forcing associated with the vertical variation of temporal and vertical derivatives of the covariance of the azimuthally averaged deviations of mass and radial pressure gradient force. The fourth term is the forcing associated with the vertical derivative of the mean torque.

The mean torque is a sum of isentropically, azimuthally–averaged mass–weighted components and is expressed by

$$\begin{aligned}\hat{F} &= \overline{\rho J_\theta F} / \overline{\rho J_\theta} \\ &= -<\frac{\partial \psi}{\partial \alpha}> + <\Gamma \cdot \bar{F}> a\sin\beta - <\Gamma \cdot [\frac{d_a \bar{W}_{oa}}{dt} - \bar{\Omega}x(\bar{\Omega}x\bar{r})]> a\sin\beta + \\ &\quad <\frac{d\bar{k}_0}{dt} \cdot \bar{g}_a> - <\bar{k}_0 \cdot (\bar{\Omega}x\bar{g}_a)> - (\frac{\partial \bar{p}}{\partial \theta})^{-1}\frac{\partial}{\partial \theta}(\frac{\partial \bar{p}}{\partial \theta} < g_{az}^* \theta^* >) \\ &\quad - (\frac{\partial \bar{p}}{\partial \theta})^{-1}\frac{1}{a\sin\beta}\frac{\partial}{\partial \beta_\theta}[\frac{\partial \bar{p}}{\partial \theta} < (u - w)_\beta^* g_{az}^* > \sin\beta].\end{aligned} \tag{4}$$

The respective components in (4) represent the forcing associated with pressure torque, frictional torque, inertial torque, the tilting of angular momentum towards or away from the local vertical axis due to a cyclone's movement over the spherical earth and the divergence of vertical and horizontal eddy angular momentum transport. All the components in (4) are expressed in terms of a mass–weighted azimuthal average (symbolized by $\wedge$ or $< >$) in order to properly account for the correlation between azimuthal variation of mass and forcing components within the asymmetric structure of baroclinic cyclones.

Relative to previous studies of the forcing of meridional circulation within a symmetric and stationary circumpolar vortex (Eliassen, 1951), a zonally averaged circumpolar vortex (Kuo, 1956; Gallimore and Johnson, 1981) and a stationary tropical vortex (Sundqvist, 1970; Challa and Pfeffer, 1980; Pfeffer and Challa, 1981; Schubert and Alworth, 1987; Molinari and Vollaro, 1990; Molinari et al., 1993), the forcing in this study includes four additional terms. The first is the inertial torque [the third term on the right in (4)] that deals with acceleration / deceleration of the storm axis with respect to an absolute framework, and centripetal acceleration relative to an asymmetric mass distribution. The second [the fourth term on the right in (4)] deals with the tilting of the local vertical axis due to the movement of cyclones over the spherical earth towards or away from the vector of absolute angular momentum $\bar{g}_a$. The third and fourth terms are associated with the tendency of the vertical derivative of a covariance between the azimuthally averaged deviations of the mass and radial pressure gradient force [term 2 on the right side of (1)], and the vertical gradient of mass–weighted azimuthally averaged diabatic heating and the second order vertical derivative of the covariance of the azimuthally averaged deviations of mass and radial pressure gradient force [term 3 on the right side of (1)]. Since these two terms involve third derivatives, their diagnoses were noisy and not feasible in this numerical study through the use of finite differencing and low spatial and temporal resolutions. Therefore these two terms were not included in the

following numerical study.

III. THE NUMERICAL SCHEME AND BOUNDARY CONDITIONS

In this numerical study, a second-order central differencing scheme and a successive-over-relaxation iteration method are applied to the flux form of (1) expressed in isentropic coordinates (Appendix A). The calculation of forcing terms and coefficients in (1) is discussed in Appendix B.

The storm volume utilized in this study is bounded laterally at a radius defined by $a\sin\beta_{max}$ with "a" representing the radius of the earth and $\beta_{\max}$ equal to 10.5° latitude. The 10.5° latitudinal arc as an equivalent radial distance from the lateral boundary to the storm axis of rotation is approximately 1000 km. Vertically, the domain is bounded by θ_S representing the earth's surface and θ_T representing an isentropic surface at the top of the troposphere.

1. *The Inner and Outer Boundary Conditions*

With $a\sin\beta$ equal to zero at $\beta=0$, the azimuthally-averaged mass-weighted radial motion $a\sin\beta(\hat{u}-\hat{w})_\beta$ vanishes at the center of the cyclone. This condition implies that the stream function S is constant at the inner boundary [see (2)].

The outer boundary conditions at β equal to 10.5° are determined partly based on the conclusion drawn by Anthes and Johnson (1968) and Sundqvist (1970) that for a tropical cyclone, the cooling must occur over an area of 1300-1400 km radius in order to balance the heating. Since the release of latent heat in the mature stage of a tropical cyclone is about 7×10^{14} watts (Malkus and Riehl, 1960; Dunn and Miller, 1964) and the estimated cooling by radiation in a tropospheric column is about 130 watts/m^2 in the tropics (Palmen and Newton, 1969), the balance between the heating and cooling does not occur in a storm volume with a lateral boundary at 1000 km. Thus, the system must be treated as open. The streamfunction S at the outer boundary is obtained based on the following relationship

$$a\sin\beta<u-w>_\beta = a\sin\beta\frac{\overline{\rho J_\theta(u-w)_\beta}}{\overline{\rho J_\theta}} = a\frac{\hat{\partial}\overline{S}}{\partial\theta}\Big/\frac{\hat{\partial}\overline{p}}{\partial\theta}, \tag{5}$$

between S and the azimuthally-averaged mass-weighted storm-relative radial motion $<u-w>_\beta$ which is obtained from diagnostic analyses of the data used in this study. In order to ensure consistency in the mass balance determined from quasi-Lagrangian diagnostics, the azimuthally-averaged lateral mass transport $\overline{\rho J_\theta(u-w)_\beta}$ at the outer boundary is adjusted. This adjustment is based on the assumption that the vertical integrated azimuthally averaged radial mass transport at the open outer boundary equals the tendency of mass within the 10.5° radius storm volume

$$\frac{\delta M}{\delta t} = -2\pi a\int_{\theta_S}^{\theta_T}[\overline{\rho J_\theta(u-w)_\beta}\sin\beta]d\theta|_{adj\ \ at\ \ \beta=10.5^\circ}, \tag{6}$$

where the total mass in the 10.5° radius storm volume is defined by

$$M = 2\pi a\int_{\theta_S}^{\theta_T}\int_{0^\circ}^{10.5^\circ}\overline{\rho J_\theta}\sin\beta\ d\beta d\theta. \tag{7}$$

The adjusted lateral mass transport $\overline{\rho J_\theta(u-w)_\beta}$ at the outer boundary is expressed by

$$2\pi a[\overline{\rho J_\theta(u-w)_\beta}\sin\beta]_{adj} = 2\pi a[\overline{\rho J_\theta(u-w)_\beta}\sin\beta] - \overline{\rho J_\theta}\hat{\delta}, \tag{8}$$

where the adjustment $\hat{\delta}$ is

$$\hat{\delta}=\{\frac{\delta M}{\delta t}+2\pi a\int_{\theta_s}^{\theta_T}\overline{\rho J_\theta(u-w)_\beta}\sin\beta]d\theta\}\,/\,\int_{\theta_s}^{\theta_T}\overline{\rho J_\theta}\,d\theta. \tag{9}$$

2.*The Lower and Upper Boundary Conditions*

At the lower boundary where isentropic surfaces intersect the earth's surface, Lorenz's (1955) convention is applied. In this convention all the properties on the " underground" isentropic surfaces ($\theta\leqq\theta_s;\theta_s$ is the surface potential temperature) are set to their respective values at the earth's surface with the exception of temperature and the Montgomery stream–function, both of which vary linearly with potential temperature. As such, both the hydrostatic mass ρJ_θ [equal to $(\Delta p/g)$] and the radial mass transport are zero in the segment of the azimuthal isentropic layer which is underground. With the vertical motion of the radial–vertical circulation in the mass coordinates (Gallimore and Johnson, 1981; Johnson and Yuan, 1998a) specified by

$$\hat{\omega}_p=\overline{(\rho J_\theta\frac{\delta p}{\delta t}+\rho J_\theta\overline{U}\cdot\nabla_\theta p+\rho J_\theta\dot{\theta}\frac{\partial p}{\partial\theta})}\,/\,\overline{\rho J_\theta}, \tag{10}$$

and ρJ_θ equal to zero everywhere in underground isentropic layer, the mean vertical motion $\hat{\omega}_p$ in the mass coordinates must vanish at the lower boundary. With this condition and the relationship between $\hat{\omega}_p$ and the stream function S in (3), S should be uniform at the lower boundary.

At the upper boundary, the variation of pressure on isentropic surfaces in time and space is much less than the variation of pressure within the troposphere. Thus, the mass weighted average of the tendency of pressure [term1 in (10)] and the advection of pressure [term 2 in (10)] are assumed to vanish. These assumptions combined with an assumption that the isentropic areally averaged diabatic mass flux [term 3 in (10)] vanishes in the stratosphere permit an assumption that $\hat{\omega}_p$ vanishes at the upper boundary. With this last assumption S must be uniform at the upper boundary. As such, setting S equal to zero on all but the outer boundary provides the system with zero mass transport at the inner, upper and lower boundaries.

IV. CASE STUDY OF EXTRATROPICAL AND TROPICAL CYCLONES

1. *The Ohio Blizzard of 25 – 27 January 1978*

(1) *Synoptic situation of the Ohio Blizzard*

The Ohio blizzard has been the focus of numerous studies since its occurrence in January 1978 (Wagner, 1978; Anthes and Keyser, 1979; Edman, 1979; Burrows et al., 1979; Salmon and Smith, 1980; Hale, 1983; Gaza and Bosart, 1990; Hakim et al., 1995, 1996). Between 1200 UTC 25 and 1200 UTC 26 January 1978, a rapid deepening of 42 hPa in 24 hours was observed in the Ohio cyclone (Fig. 1). Its central mean sea level pressure (MSLP) reached a minimum of 956 hPa. Wind gusts exceeded 100 mph and wind chill temperatures dropped to the −50° to −70° F range. Moreover, tornadoes struck Virginia, North Carolina and Florida. Two feet of snow fell in the Ohio River Valley and two inches of rain caused flooding in New England.

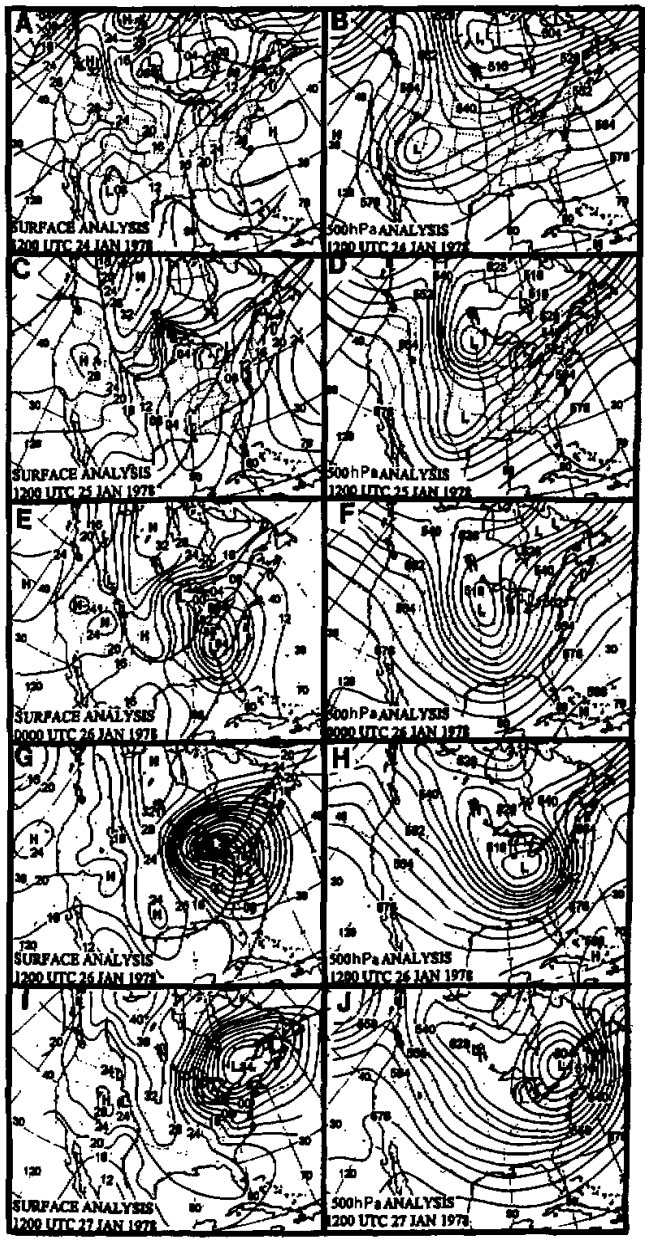

Fig. 1. Mean sea level pressure (hPa) and 500 hPa height (dekameters) analyses, respectively. (a) and (b) at 1200 UTC 24, (c) and (d) at 1200 UTC 25, (e) and (f) at 0000 UTC 26, (g) and (h) at 1200 UTC 26 and (i) and (j) at 0000 27 UTC January 1978 (from Hale, 1983).

Prior to the initial cyclogenesis of the Ohio storm, a polar short wave trough was located over the central Canada and a long wave trough was situated over the western United States. At 1200 UTC 24 January, the polar short wave in the upper troposphere moved rapidly southward as intense amplification of the long wave trough with a southwest–northeast orientation occurred (Fig. 1b). In the lower troposphere, more than half of the United States was under the influence of strong warm, moist southwesterly flow ahead of the trough. Meanwhile, the surface cold front intensified and temperature gradients strengthened (Fig. 1a).

At 1200 UTC 25 January, the long wave trough was oriented north–south over the central United States (Fig. 1d). Cold air behind the deep trough surged southward and warm subtropical air ahead of the trough moved northward. At the surface, a depression with a 998 hPa central MSLP formed along the portion of the cold front in Mississippi (Fig. 1c). Another surface low with a 1000 hPa central MSLP was located over northern Minnesota.

In a study of the jet streaks and associated ageostrophic motion and divergence at 0000 UTC 26, Edman (1979) identified three jet streaks associated with the long wave trough, a subtropical jet streak over Ohio, and polar jet streaks over Alabama and Kansas. The first and the second jets were the most intense with maximum wind speeds above 60 m s^{-1}. The interaction of these two jet streaks provided enhanced upper level divergence (Figs. 14 and 16 in Edman 1979). As a result, the southern low pressure system deepened 22 hPa in 12 hours (from 000 UTC to 1200 UTC 26) during its northeastward movement. By 1200 UTC 26 January, the third jet streak merged with the second and the northern low pressure system moved eastward and merged with the much more intense southern system. In a recent analysis of the Ohio storm, Hakim et al. (1995, 1996) emphasized that the mergence of two upper tropospheric precursor disturbances (also known as jet streaks) due to the confluence of large–scale background flow was the key contribution to the explosive growth of the system. Following the explosive development, the low pressure system occluded and became a cold core circulation with an axisymmetric structure. In the next 24 hours, the low pressure system weakened and slowly moved northeastward.

(2) *The data set*

The data prepared in the mass and angular momentum budget study of the Ohio cyclone (Hale 1983) were used in this study. The radiosonde data for the Ohio Blizzard were interpolated on a 2 × 2 degree latitude–longitude and 50 hPa grid by using Barnes (1973) method for the horizontal and linear interpolation for the vertical. These data on isobaric surfaces then were interpolated to a storm spherical isentropic coordinate system (Johnson and Downey, 1975a) with 28 levels at 5 K interval from 235 K to 370 K and seven concentric circles at radial increment equivalent to 1.5° latitudinal arc. Each circle contains 36 grid points surrounding the storm center at radii equivalent to 1.5°, 3.0°, 4.5°, 6.0°, 7.5°, 9.0° and 10.5° latitudinal arc.

(3) *The forcing of the radial–vertical circulation within the Ohio Blizzard: diagnostic results and discussions*

In a previous mass and angular momentum budget study of the Ohio cyclone utilizing quasi–Lagrangian diagnostics, Hale (1983) showed that the intensity of its azimuthally–averaged radial–vertical mass circulation with strong mass convergence in the lower isentropic layers and divergence in the upper isentropic layers was approximately twice that of other cyclones examined in a series of quasi–Lagrangian analyses (Adrian, 1981; Johnson and

Downey, 1976; Johnson et al., 1976; Wash, 1978; Rosinski, 1983; Johnson and Hill, 1987). The strong inward transport of angular momentum by the inward branch of the isentropic mass circulation induced low-level rotation and an S-shaped deformation of the low-level baroclinic structure. A concurrent adjustment of the flow in the upper troposphere associated with the self-development process (Sutcliffe, 1947; Palmen and Newton, 1969; Johnson and Hill, 1987) occurred in response to the low-level S-shaped baroclinic structure through the thermal wind. As a result, strong eddy angular momentum convergence occurred in the upper troposphere. This self-development process combined with the upward diabatic transport of angular momentum due to intense latent heat release contributed to the cyclogenesis throughout the troposphere.

Hale's results confirmed the conclusion drawn from previous studies (Johnson and Downey 1975 a, b; Johnson and Downey 1976) that a net outward transport of mass and a net inward transport of absolute angular momentum are required for the development and maintenance of cyclones. This mass and angular momentum transport is accomplished through a systematic radial-vertical mass circulation within cyclones (Johnson and Downey, 1975a).

The numerically simulated and " observed" azimuthally-averaged mass-weighted radial-vertical circulation for the Ohio cyclone are now compared. The simulated azimuthally-averaged mass-weighted radial motions at radii equivalent to 1.5°, 3.0°, 4.5°, 6.0°, 7.5° and 9.0° latitudinal arcs were obtained numerically through solving (1). Only the results for radius of 7.5° are shown here (dashed lines in Fig. 2) in order to compare directly with the results from the previous angular momentum budget study of the Ohio cyclone (Hale 1983). In Fig. 2, the solid lines display the " observed" azimuthally-averaged mass-weighted radial motions obtained from the direct diagnoses of the data used in this study. The negative (positive) value in each panel of Fig. 2 represents systematic inward (outward) mass transport. These profiles in each panel agree quite well, although some disparities exist in magnitude. These disparities involve data and truncation errors and errors from the calculations of the open outer boundary condition, diabatic heating or frictional torque and the assumptions utilized in developing the theory for the balanced vortex.

Since the simulated and observed results shown in Fig. 2 are in good agreement, the linearity of the diagnostic equation enables systematic assessment of relative importance of internal physical processes in forcing the radial motion within cyclones. This assessment is performed first by simply comparing the orders of magnitude of the forcing components (Table 1), and then by comparing the components of simulated radial motion in response to individual internal forcing.

Table 1 lists the maximum orders of magnitude of seven forcing components along with the ranges of the order of magnitude of hydrodynamic stability at every time period for the radius of 7.5°. The comparison based on Table 1 shows that pressure torque and eddy angular momentum are dominant factors. The maximum magnitudes of the forcing terms associated with pressure torque (column 2) and eddy angular momentum transport (column 5) are one order larger than those of the forcing terms associated with diabatic heating (column 3) and the tilting of angular momentum towards or away from the local vertical axis due to the cyclone's movement over the spherical earth (column 7). Although the maximum orders of magnitude of the forcing terms associated with the divergence of the vertical eddy angular momentum transport (column 4) and inertial torque (column 6) at some periods of time are as large as those of the forcing terms associated with pressure torque (column 2) and the horizontal eddy angular momentum transport (column 5), the vertical distributions of the forcing

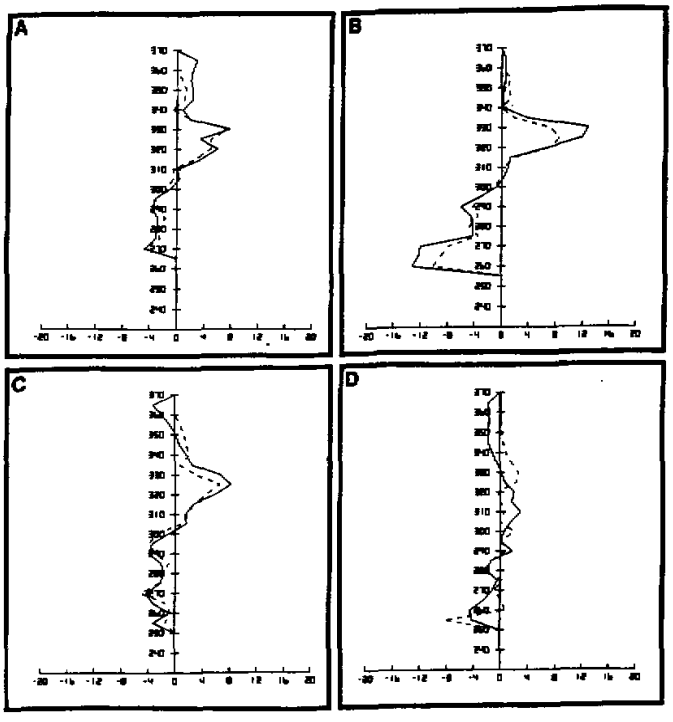

Fig. 2. Vertical profiles of simulated (dashed) and diagnosed (solid) azimuthally–averaged mass–weighted radial motion (m s^{-1}outflow positive) for the radius of 7.5° within the Ohio cyclone at (a) 1200 UTC 25, (b) 0000 UTC 26, (c) 1200 UTC 26 and (d) 0000 UTC 27 January 1978.

terms associated with pressure torque and the horizontal eddy angular momentum transport are more regular. For instance, the maximum order of magnitude of 10^{-11} for the latter two terms occurs in a deeper layer relative to those of terms associated with vertical eddy transport (column 4) and inertial torque (column 6).

The comparisons of the components of simulated radial motion in response to internal forcing terms are presented in following five subsections. Note that the simulated radial motion obtained from solving (1) in response to individual internal forcing includes the trade off between the forcing and stability. Each component of simulated radial motion associated with each individual internal forcing does not include the effect of outer boundary condition.

(i) *The effect of pressure torque*

Since the pressure torque is uniquely related to the radial geostrophic mass transport (Johnson and Downey, 1975b; Johnson and Yuan, 1998a)

$$\text{pressure torque} = -<\frac{\partial \psi}{\partial \alpha}> = \overline{\rho J_\theta f a \sin\beta (u_g)_\beta} \,/\, (\overline{\rho J_\theta}), \tag{11}$$

inward (negative) and outward (positive) geostrophic mass transports are equivalent with negative and positive pressure torques respectively. Fig. 3 displays the distribution of the

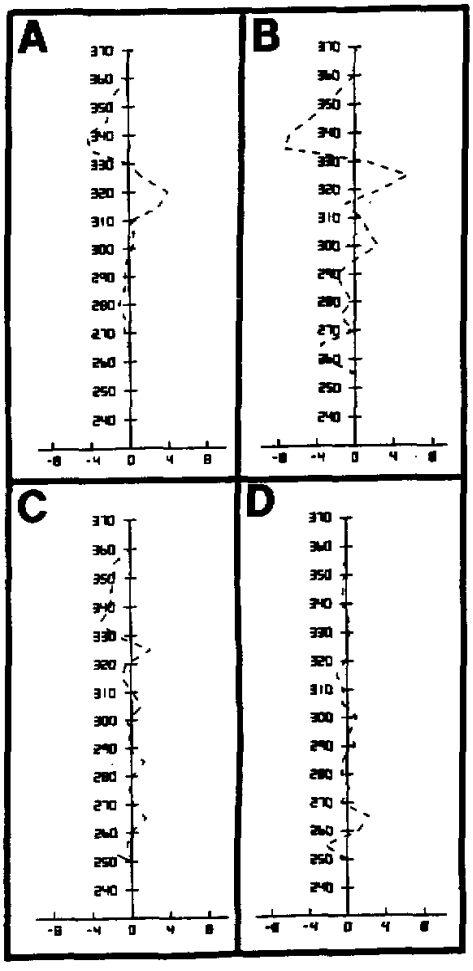

Fig. 3. Vertical profiles of simulated azimuthally–averaged mass–weighted radial motion ($m\ s^{-1}$ outflow positive) forced by pressure torque for the radius of 7.5° within the Ohio cyclone at (a) 1200 UTC 25, (b) 0000 UTC 26, (c) 1200 UTC 26 and (d) 0000 UTC 27 January 1978.

azimuthally–averaged mass–weighted radial motion forced by pressure torque for the radius of 7.5° in isentropic coordinate. This distribution of radial motion in general is consistent with the distribution of areally integrated mass weighted pressure torque in the isentropic time section for the radius of 7.5° from Hale's budget study of the Ohio cyclone (Fig. 4).

During the first half of development (Figs. 3a, b), a three–layer structure of radial motion forced by pressure torque can be identified. The inward transport in higher and lower valued isentropic layers forced by negative pressure torque and outward transport in the middle isentropic layers forced by positive torque are intensifying at 0000 UTC 26. At this time, the 295 – 330 K outflow in Fig. 3b is forced by positive pressure torque [focus on 0000 UTC 26 (2600) in Fig. 4] which is associated with the strong geostrophic component of the

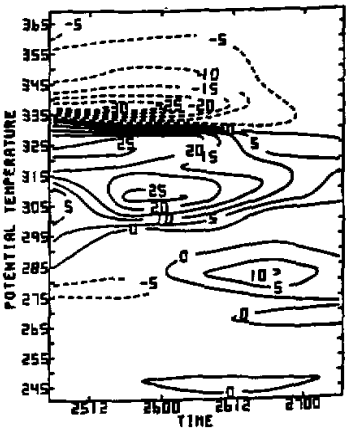

Fig. 4. Isentropic time section of area integral of mass weighted pressure torque (10^{16}kg m^{2}s^{-2}) within a circular area with radius of 7.5° latitudinal arc (Hale, 1983).

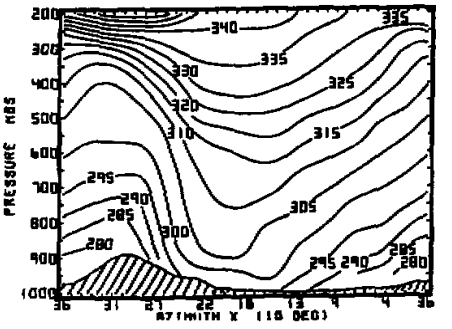

Fig. 5. Azimuthal–vertical distribution of potential temperature for the radius of 7.5° within the Ohio cyclone at 0000 UTC 26 January 1978 (from Hale, 1983).

southwesterly flow to the northeast of the storm center where the hydrostatic mass is large in a region of low static stability (Figs. 5, 6a). The 330 – 360 K inflow in Fig. 3b is forced by negative pressure torque (Fig. 4) associated with the subtropical jet and the largest amount of hydrostatic mass in the southwestern quadrant of the storm volume (Figs. 5, 6b). The lower level inflow is forced by negative pressure torque (Fig. 3b, 4). The inward branches of the radial–vertical mass circulation, which transport storm angular momentum towards the axis of rotation (Johnson et al., 1976; Hale, 1983; Johnson, 1988), are responsible for the development of maxima specific relative angular momentum $(u - w)_a a \sin\beta$ in higher valued isentropic layers around 340 K and lower valued isentropic layers around 280 K (Fig. 7). According to the results from previous angular momentum budget studies of the Ohio cyclone (Johnson et al., 1976; Hale, 1983; Johnson, 1988), the increase of angular momentum in middle isentropic layers occurs partly through the transfer of angular momentum by pressure stresses from higher and lower valued isentropic layers to the middle layers. These pressure stresses are intrinsically coupled with the negative torques in the higher and lower valued isentropic layers and positive torque in middle isentropic layers. As the storm occludes, the increase in symmetry leads to a decrease in the intensity of the radial motion forced by pressure torque (Figs. 3c, d).

(ii) *The effect of horizontal and vertical eddy angular momentum transports*

Although eddy angular momentum convergence is not an absolute torque within the azimuthally–averaged structure, in effect it is equivalent with a "torque" since storm angular momentum decreases or increases due to its action. In its primitive form, this mode stands for a non–linear baroclinically forced convergence of angular momentum associated with a well defined upper–level S–shaped wind pattern which results from the adjustment of upper atmospheric flow to the low–level counterpart patterns of the baroclinic temperature structure and thermal wind (Wash, 1978; Johnson and Hill, 1987; Johnson, 1981). The radial motion within the Ohio Blizzard forced by the horizontal eddy mode, is displayed in Fig. 8.

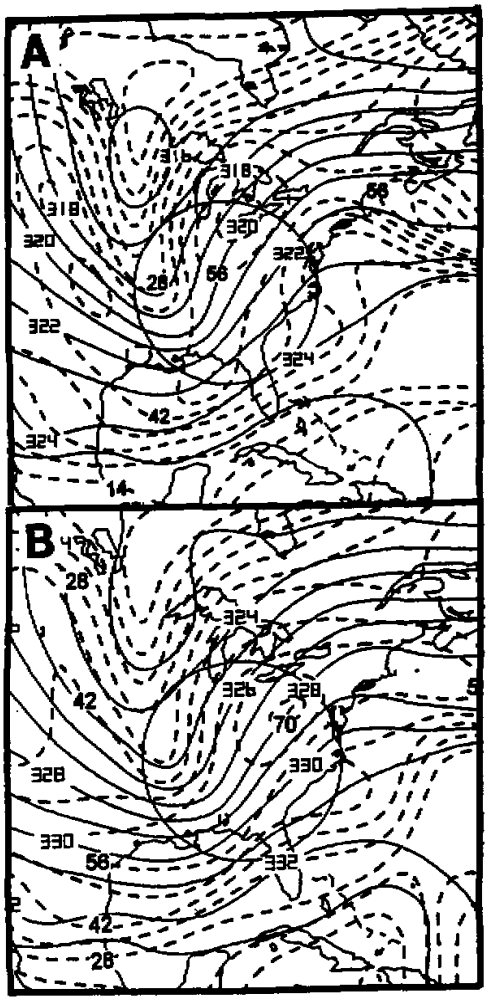

Fig. 6. Montgomery stream function (m^2s^{-2}) and isotaches ($m\ s^{-1}$) for the Ohio cyclone. (a) 325 K at 0000 UTC 26 and (b) 335 K at 0000 UTC 26 January 1978. The circle with the radius equivalent to 7.5° latitudinal arc represents the position of the quasi-Lagrangian storm volume.

$$-\left(\frac{\partial \overline{p}}{\partial \theta}\right)^{-1}\frac{1}{a\sin\beta}\frac{\partial}{\partial \beta}\left[\overline{\frac{\partial p}{\partial \theta}(u-w)^{*}\beta g_{az}^{*}\sin\beta}\right], \tag{12}$$

During the first half of development (Fig. 8b), this mode results in the outflow around 340 K which is offset by the inflow forced by negative pressure torque (Fig. 3b). The distribution of outward mass transport during the second half of development (Fig. 8c) is consistent with the 325 K mass divergence at 1200 UTC 26 in Edman's study of the Ohio cyclone (Fig. 16 in Edman, 1979) and with the distribution of positive horizontal eddy mode in Hale's study (Fig. 20b in Hale, 1983). A comparison of the intensity of the forced components of the radial motion in Figs. 3c and 8c suggests that the effect of the horizontal eddy mode

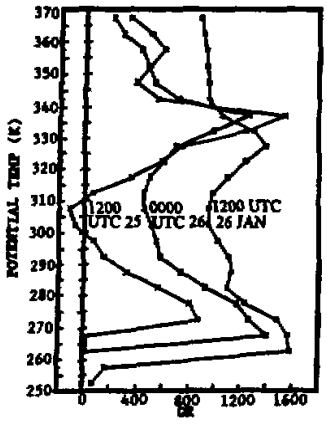

Fig. 7. Vertical profiles of area–averaged specific relative angular momentum for the Ohio cyclone of 25–26 January 1978 ($10^4 m^2 s^{-1}$) within a quasi–Lagrangian storm volume equivalent to 7.5° latitudinal arc (from Johnson, 1988).

within the Ohio Blizzard persists longer than that of pressure torque. After 1200 UTC 26, the outflow forced by the horizontal eddy mode decreases as the system became more symmetric (Fig. 8d).

The isentropic time section of total (mean and eddy) lateral absolute angular momentum transport (Fig. 9) for the radius of 7.5° shows that at 0000 UTC 26, inward transport (positive) occurs in the layers below 315 K and in the layer from 335 K to 365 K. Outward transport occurs in the layer from 315 K to 335 K. Since the inward branch of mass circulation carries more absolute angular momentum toward the axis of the rotation than the outward branch removes due to the azimuthally–averaged absolute angular momentum increasing with radius (Fig. 3 in Johnson and Hill, 1987), the net inward lateral absolute angular momentum transport shown in Fig. 9 leads to the spin up of the cyclone vortex. The spin up of the circulation in the 315 K and 335 K layer shown in Fig. 7 stems from the storm angular momentum transfer from lower and higher value isentropic layers to the middle layer by pressure stress, upward diabatic angular momentum transport and the net convergence of positive eddy angular momentum transport.

The asymmetric structure of the system also impacts the radial motion through the vertical eddy angular momentum transport $(\partial\overline{p}/\partial\theta)\partial[(\partial\overline{p}/\partial\theta)<\dot{\theta}^{*} g_{az}^{*}>]/\partial\theta$. In the present study, the radial motion forced by the vertical eddy mode at 0000 UTC 26 for the radius of 7.5° is not as intense as that for smaller radii of 1.5°, 3.0° and 4.5° (Figs. 10a, b). The reason is likely that the heating rate and the radial gradient of latent heat release are more intense and asymmetric at smaller radii than at the radius of 7.5° (Fig.18 in Hale, 1983).

(iii) *The effect of the inertial torque*

The inertial torque defined in absolute coordinates is now expressed in earth–relative coordinates

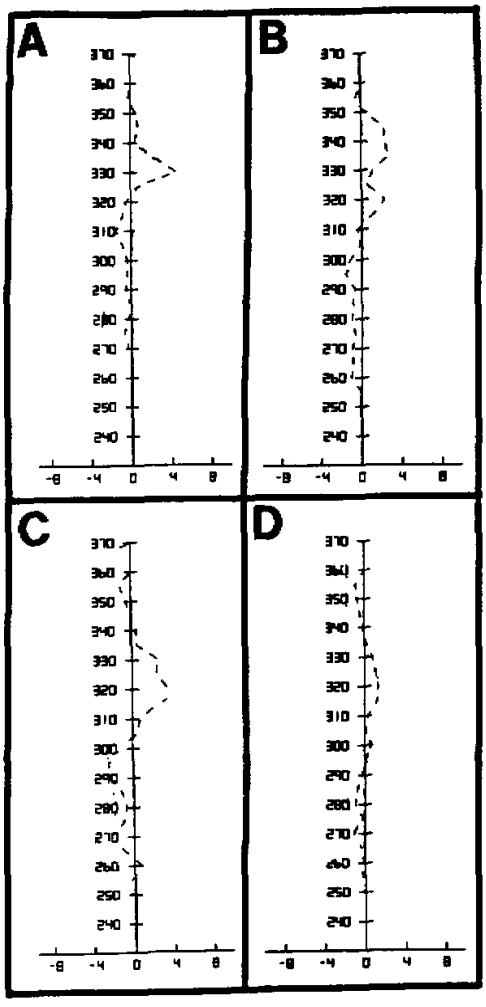

Fig. 8. Vertical profiles of simulated azimuthally-averaged mass-weighted radial motion ($m\ s^{-1}$ outflow positive) forced by horizontal eddy mode for the radius of 7.5° within the Ohio cyclone at (a) 1200 UTC 25, (b) 0000 UTC 26, (c) 1200 UTC 26 and (d) 0000 UTC 27 January 1978.

$$\text{inertial torque} = -\langle \Gamma \cdot \frac{d\bar{W}_0}{dt} \rangle a\sin\beta - \langle \Gamma \cdot (2\bar{\Omega} x \bar{W}_0) \rangle a\sin\beta + \langle \Gamma \cdot \{\bar{\Omega} x [\bar{\Omega} \times (\bar{r} - \bar{r}_0)]\} \rangle a\sin\beta. \quad (13)$$

The forced radial motion by inertial torque represents the net storm relative mass transport due to the movement of a storm system in an asymmetric mass field. The velocity of the storm volume $\bar{W}_0$ and its acceleration were determined from 12-hour positions of the storm's central pressure. In (13) the third term is cancelled by a corresponding forcing term associated with the tilting of storm angular momentum towards or away from the local vertical axis [see

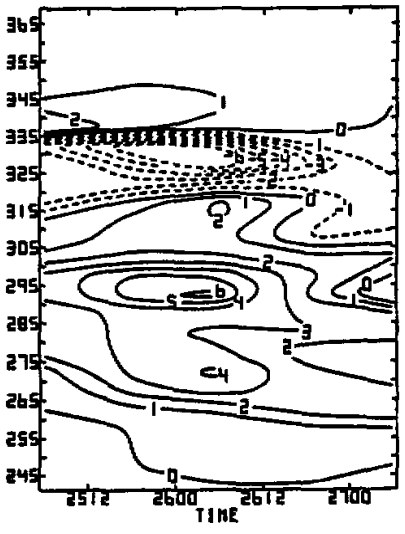

Fig. 9. Isentropic time section of total lateral angular momentum transport (10^{-17}kg m^{2}s^{-2} positive value for inward transport) for the radius of 7.5° within the Ohio cyclone (from Hale, 1983).

(47) in Johnson and Yuan, 1998a]. In addition, the results of the present study indicate that the first term is one order of magnitude smaller than the second term in (13), since the acceleration of the storm velocity is minimal at this stage (Fig. 11). Thus, the following analysis will focus on the second term in (13).

The second term is associated with the azimuthally averaged mass–weighted azimuthal component of Coriolis force in terms of storm velocity. Since the azimuthal unit vector $\vec{T}$ is directed counterclockwise, the azimuthal component of Coriolis force associated with the storm velocity is negative (resulting in inflow) in the leading half of the storm volume and positive (resulting in outflow) in the trailing half of the volume. At 0000 UTC 26 the storm moved north–northeastward. Thus inflow occurs in the north–northeastern half of the volume and outflow in the south–southwestern half of the volume. The azimuthally–averaged mass–weighted inflow around 270 K in Fig. 12 is associated with more mass in the leading half of the storm volume (Fig. 13a). The outflow around 275 K in Fig. 12 is associated with more mass in the trailing half of the volume (Fig. 13b). The weak static stability with more mass within the isentropic layer in the leading half of the storm volume (Fig. 13c) is responsible for the inflow around 300 K in Fig. 12. Above 315 K, the inflow and outflow are associated with subtropical flows shown in Figs. 13d and 13e respectively. With the storm occlusion, mass distribution became more axisymmetric and the effect of this inertial torque on the radial motion decreases.

The effect of the tilting term $< (\vec{W}_0 \cdot \vec{g}_a)/r_0 > - < \vec{k}_0 \cdot (\vec{\Omega} \times \vec{g}_a) >$ on the radial motion is very small compared with other forcing terms and hence is not included in this discussion.

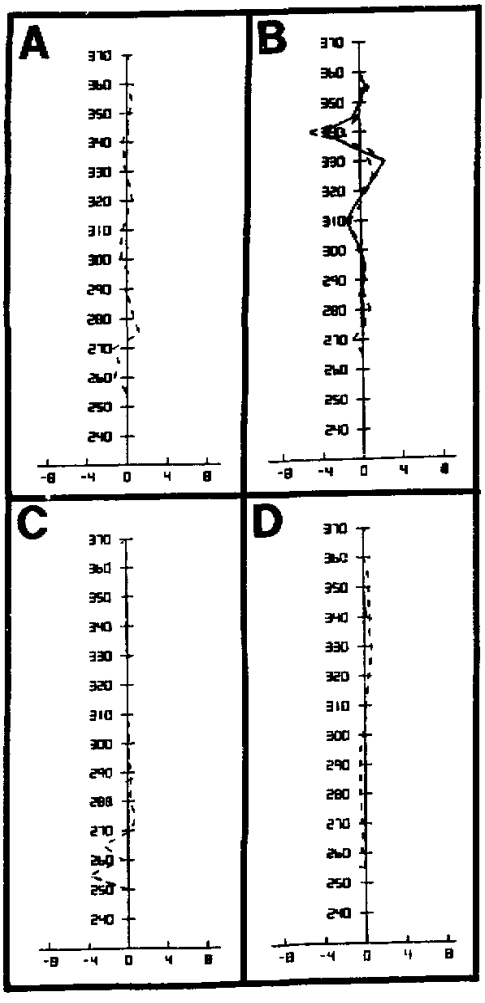

Fig. 10. Vertical profiles of simulated azimuthally-averaged mass-weighted radial motion (m s^{-1} outflow positive) forced by vertical eddy mode (a) for the radius of 7.5° at 0000 UTC 26, (b) for the radii of 1.5° (thin dashed) and 3.0° (thick dashed) at 0000 UTC 26, (c) simulated azimuthally-averaged mass-weighted radial motion (m s^{-1} outflow positive) forced by frictional torque with the drag coefficient $c^2 = 0.9 \times 10^{-3}$ at 0000 UTC 27 for the radius of 7.5° and (d) simulated meridional motion associated with diabatic heating at 0000 UTC 26 January 1978 for the radius of 7.5° within the Ohio cyclone.

(iv) *The effect of frictional torque*

The radial motion forced by frictional torque is inward in lower valued isentropic layers. The drag coefficient used in the calculation of the fricitonal torque is 0.9×10^{-3} which is close to the lowest value (1×10^{-3}) suggested by Anthes and Keyser (1979) in their simulations of

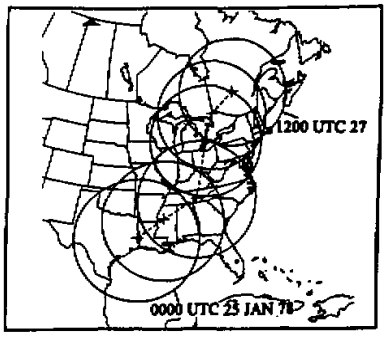

Fig. 11. Positions of the 7.5° storm volume at 12 hour intervals from 0000 UTC 25 to 1200 UTC 27 January 1978 for the Ohio cyclone (from Hale, 1983).

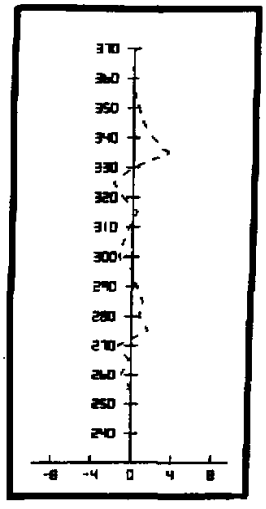

Fig. 12. Vertical profile of simulated azimuthally–averaged mass–weighted motion (m s^{-1} outflow positive) forced by inertial torque for the radius of 7.5° within the Ohio cyclone at 0000 UTC 26 January 1978.

the Ohio Blizzard with a fine–mesh model. As the storm intensifies the inflow in lower isentropic layers forced by negative frictional torque increases with time and reaches a maximum value at 0000 UTC 27 (Fig. 10c).

(v) *The effect of diabatic heating*

Figure 14 presents the vertical–radial distribution of azimuthally–averaged mass–weighted diabatic heating (K day^{-1}) which represents the vertical branch of the radial–vertical circulation in isentropic coordinates at 12–hour interval for the time period from 0000 UTC 25 to 1200 UTC 26. During the explosive growth phase, the vertical branch of the radial–vertical circulation associated primarily with latent heat release intensifies and becomes well organized. These features are consistent with the simplified composite radar charts presented by Hale (Fig. 8 in Hale, 1983). Hale's study showed that the areally averaged diabatic heating rate was two to three times larger than those in previous case studies of extratropical cyclones (Johnson and Downey, 1976; Johnson et al., 1976).

The corresponding radial motion associated with latent heat release is obtained by solving the linear diagnostic equation with only the first forcing term on the right hand side of (1). Figure 10d indicates that inflow occurs in the lower valued isentropic layers and outflow in the higher valued isentropic layers, a distribution in agreement with the heating distribution in Fig. 14b.

According to Johnson and Downey (1976), upward angular momentum transport is associated with latent heat release. The budget study of specific angular momentum (Fig. 15) shows that the large positive tendency around 325 K is primarily due to the upward diabatic transport of angular momentum and partly due to the pressure torque. The magnitude of the specific absolute angular momentum tendency within the Ohio cyclone is twice that of other

cyclones (Wash, 1978; Adrian, 1981).

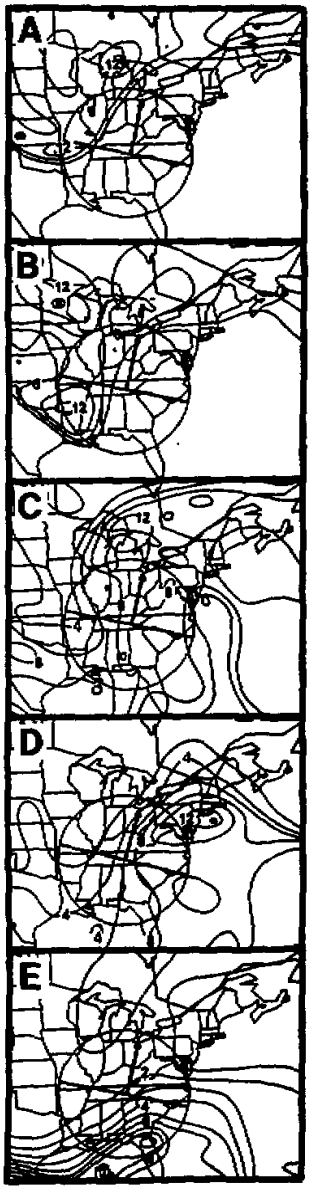

Fig. 13. Hydrostatic mass distribution (10^2kg m^{-2}) for the Ohio cyclone on (a) 270 K (b) 275 K (c) 300 K. (d) 325 K and (e) 335 K isentropic surfaces at 0000 UTC 26 January 1978. The circle with the radius equivalent to 7.5° latitudinal arc represents the position of the quasi-Lagrangian storm volume.

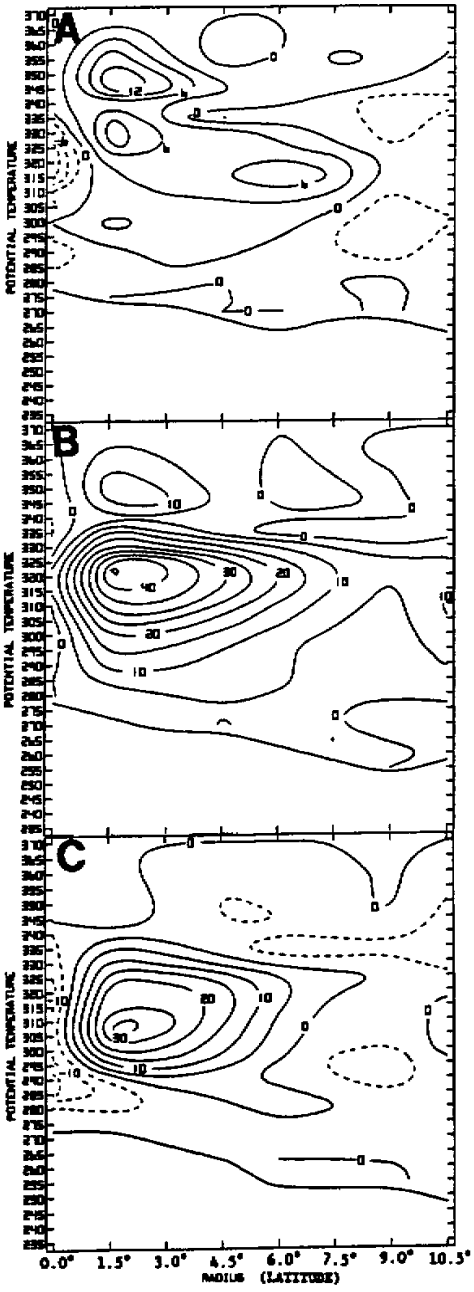

Fig. 14. The vertical–radial distribution of azimuthally–averaged mass–weighted diabatic heating (K day^{-1}) for the Ohio cyclone (a) 0000–1200 UTC 25, (b) 1200 UTC 25–0000 UTC 26, and (c) 0000–1200 UTC 26, January 1978.

(4) *Summary*

In a previous mass and angular momentum budget study of the Ohio cyclone utilizing quasi–Lagrangian diagnostics, Hale (1983) showed that the mean radial–vertical mass circulation with strong convergence of mass in the lower valued isentropic layers and divergence in the higher valued isentropic layers was more intense within the Ohio cyclone than within other cyclones. The strong inward transport of angular momentum by the mass circulation induced low–level rotation and an S–shaped deformation of the low–level temperature distribution with the concurrent adjustment of upper–level flow through the resulting thermal wind and self–development process (Sutcliffe, 1947; Palmen and Newton, 1969; Johnson and Hill, 1987). As a result, strong eddy angular momentum convergence occurred in higher valued isentropic layers. This self–development process combined with the upward diabatic angular momentum transport due to intense heating and the angular momentum transfer due to pressure stresses induced the extreme development observed in the Ohio cyclone.

Hale's study and results presented here confirm the conclusion drawn by Johnson and Downey (1975 a, b; 1976) that cyclone development requires a net divergence of mass and net convergence of storm absolute angular momentum. These requirements are fulfilled through the lateral transport of these properties within the Ohio cyclone. During the first half of development, the dominent internal forcing is associated with pressure torque. Storm absolute angular momentum is transported into the system mainly through the forced inward mass transport by negative pressure torques in the lower and higher valued isentropic layers linked with the polar jet and also with the subtropical jet. For example, at 0000 UTC 26 at 265 K, 4 m s^{-1} inflow is forced by negative pressure torque (Fig. 3b), which accounts for almost half of the maximum total inflow of 9 m s^{-1} (dashed line in Fig. 2b). In addition to the dominent pressure torque, horizontal eddy mode accounts for 1 m s^{-1} inflow (Fig. 8b at 265 K) and outer boundary effect for 4 m s^{-1} inflow (Fig. 16 at 265 K) which is the homogeneous solution of (1) with open outer boundary conditions. The major contributors to the maximum total outflow of 9 m s^{-1} at 325 K at 0000 UTC 26 (dashed line in Fig. 2b) are pressure torque (5.5 m s^{-1} outflow in Fig. 3b), horizontal eddy mode (1 m s^{-1} outflow in Fig. 8b), outer boundary effect (3.5 m s^{-1} outflow in Fig. 16) and inertial torque (2 m s^{-1} inflow in Fig. 12). During the second half of development, the effect of pressure torque diminishes very quickly due to the occlusion and the symmetry structure of the cyclone. Horizontal eddy mode becomes the dominant internal process in the forcing of the radial motion.

Since the mean mode of storm absolute angular momentum transport is outward in the middle isentropic layer, the occlusion of the Ohio cyclone is due to the upward transport of absolute angular momentum by diabatic heating and nonconvective transfer of absolute angular momentum from lower and higher valued isentropic layers (with negative pressure torques) into the middle isentropic layer (with positive pressure torque) by pressure stresses acting on inclined isentropic surfaces within the asymmetric baroclinic structure.

2. *The typhoon Nancy of 18–23 September 1979*

(1) *Synoptic situation*

For a comparison of the forcing within extratropical and tropical cyclones, typhoon Nancy of 18–23 September 1979 is selected for the present numerical simulation (Fig. 17). This typhoon occurred over the South China Sea where the sea surface temperatures (SST) around 26.5°C were quite uniform and warm (300 K shown in Fig. 17a). Prior to the

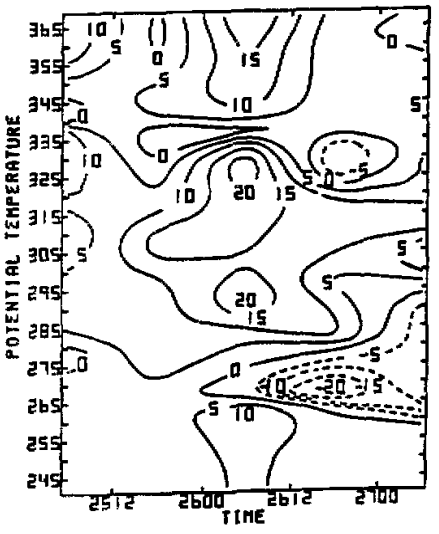

Fig. 15. Isentropic time section of specific absolute angular momentum tendency (10 m^2s^{-2}) for the radius of 7.5° within the Ohio cyclone (from Hale, 1983).

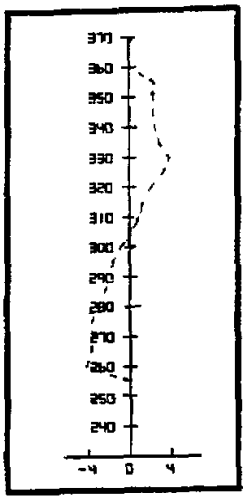

Fig. 16 Vertical profile of azimuthally-averaged mass-weighted radial motion ($m\ s^{-1}$ outflow positive) obtained from the homogeneous solution of the linear equation with open outer boundary condition for the radius of 7.5° within the Ohio cyclone at 0000 UTC 26 January 1978.

formation of typhoon Nancy within this region, a cross-equatorial current from the Southern Hemisphere to the South China Sea already existed on the 300 K isentropic surface. The cross-equatorial current interacted with easterlies to form an intertropical convergence zone (ITCZ, dashed in Fig. 17b) over the South China Sea at 0000 UTC 18 September. A disturbance (easterly wave, thick solid arrows in Fig. 17c) embedded in the easterlies on 320 K surface was evident. Above 320 K, a warm and broad anticyclone as revealed by the Montgomery stream function on 350 K dominated Southeastern Asia (Fig. 17d).

Twelve hours later by 1200 UTC 18 September, a cyclonic rotation of the 320 K wind field developed in the southern portion of the easterly wave, while a closed circulation over Philippines represented by 320 K Montgomery stream function indicated the approach of the typhoon Mac (Fig. 17g and the right storm track in Fig. 18). The same feature was evident on 300 K (Fig. 17f). Notice to the west of the easterly wave that the western portion of the ITCZ was bent towards the southwest. Around this bending point at 0000 UTC 19 September, a relatively axisymmetric closed circulation appeared in the 300 K and 320 K Montgomery stream function fields (Figs. 17j, k). In higher valued isentropic layers, the anticyclone as revealed by the Montgomery stream function on 350 K strengthened to the east and west of the storm center (Fig. 17L). The transformation from a tropical cyclone to the typhoon Nancy at 1200 UTC 19 September (represented by dashed line of the left storm track in Fig. 18) involved the effects of the warm SST within the ITCZ, a middle-layer easterly wave, a warm and broad upper-layer anticyclone, weak vertical shear of horizontal wind (Fig. 19) and

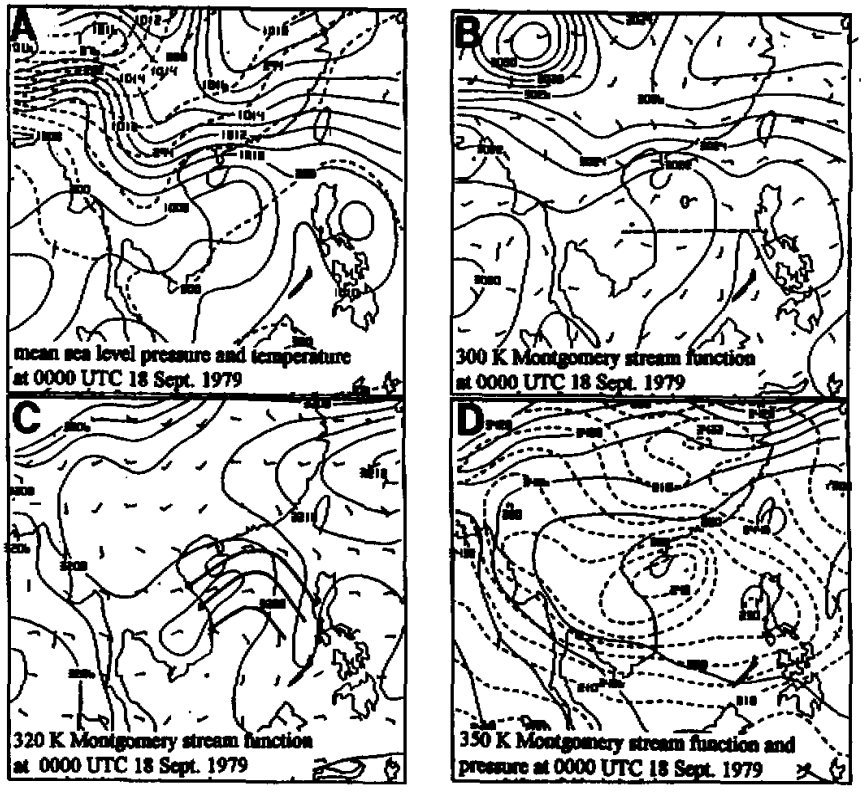

Fig. 17. Analyses of (a) mean sea level pressure (solid in hPa) and temperature (dashed in K), (b) Montgomery stream function (solid in 10^2 m^2s^{-2}) and convergence zone (dashed) on 300 K, (c) Montgomery steam function (solid) and stream line (thick solid) on 320 K and (d) Montgomery stream function (solid) and pressure (dashed) on 350 K at 0000 UTC 18 September 1979.

possibly the interaction with typhoon Mac. Typhoon Mac became a tropical cyclone after the formation of typhoon Nancy (represented by dotted line of the right storm track in Fig. 18).

Three hours later (1800 UTC 19 September), typhoon Nancy reached Hainan Island (Fig. 18) with maximum wind speeds above 40 m s^{-1} and precipitation in excess of 650 mm. Later on, typhoon Nancy moved southwestward to the southern edge of Hainan Island, then it moved westward along the south coast line of Hainan Island. From 0000 UTC 22 to 0000 UTC 23 September, typhoon Nancy moved towards the southwest and dissipated after striking Vietnam.

(2) *Data set*

The original isobaric data set available every 12 hours was the ECMWF FGGE level IIIb on a 1.875 × 1.875 lat / long grid. To obtain the isentropic data set with a vertical resolution of 10 K interval on storm spherical rings, a linear vertical interpolation with p^{κ} from isobaric to isentropic coordinates was carried out along with a horizontal interpolation from

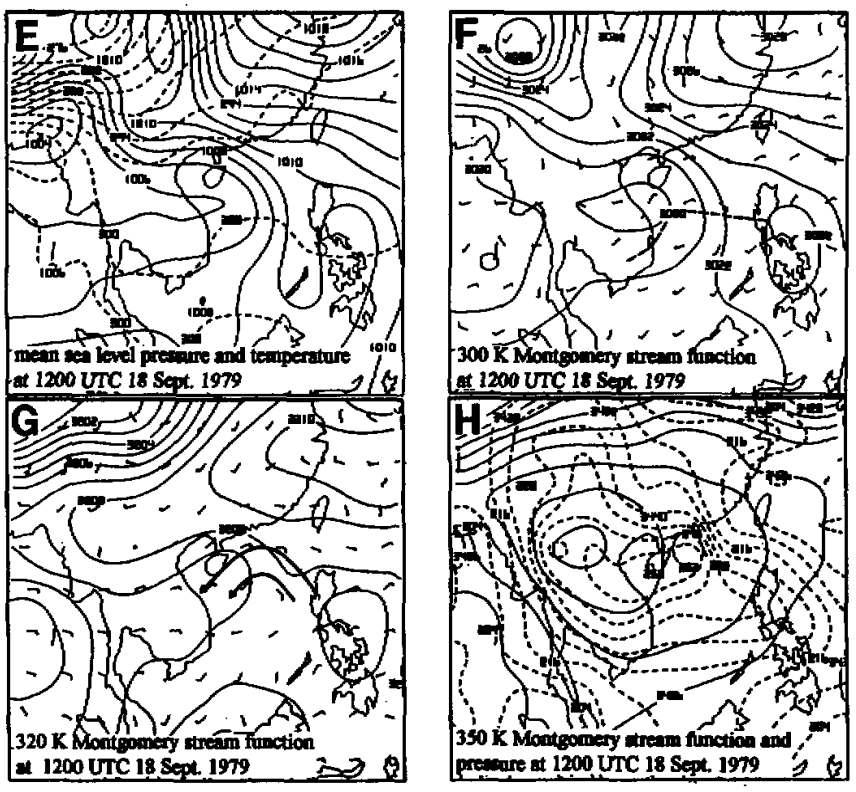

Fig. 17. (e)–(h) as (a)–(d) respectively except at 1200 UTC 18 September, 1979.

lat / long grid to storm spherical coordinates based on the methods developed by Johnson and Downey (1975a).

(3) *The forcing of the radial–vertical circulation within typhoon nancy: results and discussion*

The forced azimuthally–averaged mass–weighted radial motion within typhoon Nancy was also obtained from solving (1) utilizing open outer lateral boundary conditions and the diagnostically determined components of forcing. Since the horizontal scale of typhoon Nancy is smaller than that of the Ohio cyclone, results for 6.0° latitude storm volume are shown in Fig. 20 for the period from 1200 UTC 18 to 0000 UTC 22 September 1979. Figure 20 shows that 1) vertical distributions of the simulated radial motion (dashed) and observed (solid) radial motion which is a directly diagnosed result from the data set used for this study are in close agreement for all time periods, 2) the simulated radial motions for all time periods are slightly stronger than the observed radial motions and 3) after 1200 UTC 18 September, the two–layer structure with inflow in lower valued isentropic layers and outflow in higher valued isentropic layers is pronounced in both simulated and observed profiles of radial motion.

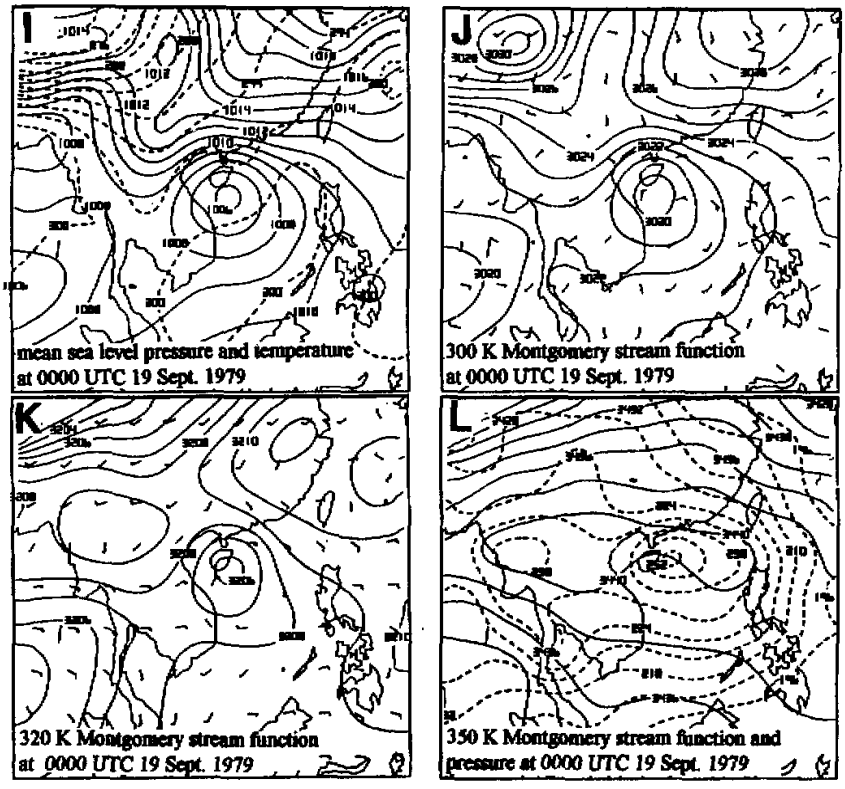

Fig. 17. (I)–(L) as (a)–(d) respectively except at 0000 UTC 19 September, 1979.

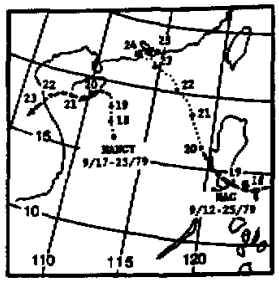

Fig. 18. Storm track from 0000 UTC 18–0000 UTC 23 September, 1979.

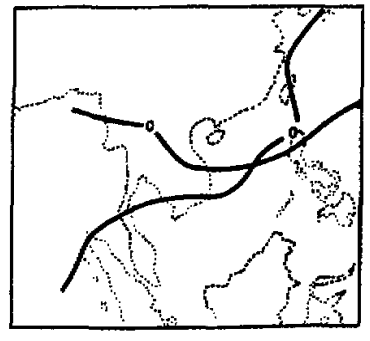

Fig. 19. Contours of zero vertical shear of horizontal wind ($u_{200}-u_{850}$, $v_{200}-v_{850}$ both shown as solid lines) for typhoon Nancy at 0000 UTC 19 September 1979.

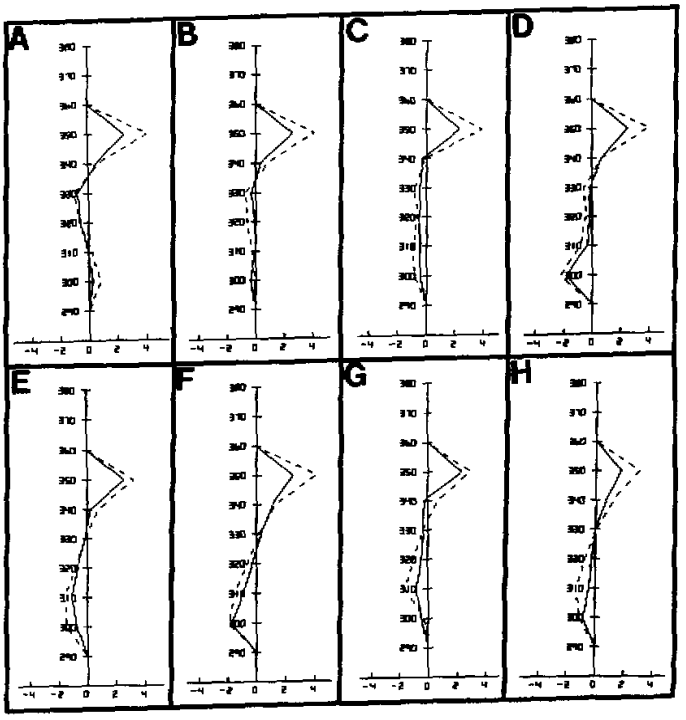

Fig. 20. Vertical profiles of simulated (dashed) and diagnosed (solid) azimuthally–averaged mass–weighted radial motion (m s^{-1}outflow positive) for the radius of 6.0° within typhoon Nancy at (a) 1200 UTC 18, (b) 0000 UTC 19, (c) 1200 UTC 19, (d) 0000 UTC 20, (e) 1200 UTC 20, (f) 0000 UTC 21, (g) 1200 UTC 21 and (h) 0000 UTC 22 September 1979.

The relative importance of stability, diabatic heating and torques within the Ohio extratropical cyclone and typhoon Nancy in terms of order of magnitude (Table 1 and 2) is now compared prior to the presentation of the simulated results from the numerical solution of (1). Table 2 shows that the minimum magnitude of stability (column 1) is one order of magnitude smaller throughout the life cycle of typhoon Nancy than in the Ohio extratropical cyclone (column 1 in Table 1). The dominant forcing responsible for the development of the radial motion within typhoon Nancy is the forcing associated with diabatic heating (column 3 in Table 2) in contrast with the dominant forcing associated with pressure torque (column 2 in Table 1) within the Ohio cyclone. Although Table 2 shows that the order of the magnitude of other forcing terms is as large as that of the diabatic forcing for a few periods of time, the vertical distribution of the diabatic forcing is more organized with a maximum order of magnitude of 10^{-13} throughout a deeper layer compared with those of other forcing terms. For example, at 1200 UTC 18 September 1979 the diabatic forcing with the large order of magnitude of 10^{-13} occurs in all but one lower level. In contrast, the forcing associated with pressure torque (column 2) is one or several orders of magnitude smaller than 10^{-13} in all but one level. The forcing associated with the divergence of vertical eddy angular momentum transport (column 4) and inertial torque (column 6) with the large order of magnitude of 10^{-13} is also

restricted to thin layers.

Now, the relatively important role of hydrodynamic stability and individual internal forcing in relation to each other in forcing the radial–vertical circulation within typhoon Nancy is examined based on the results obtained from solving (1) with closed outer boundary conditions.

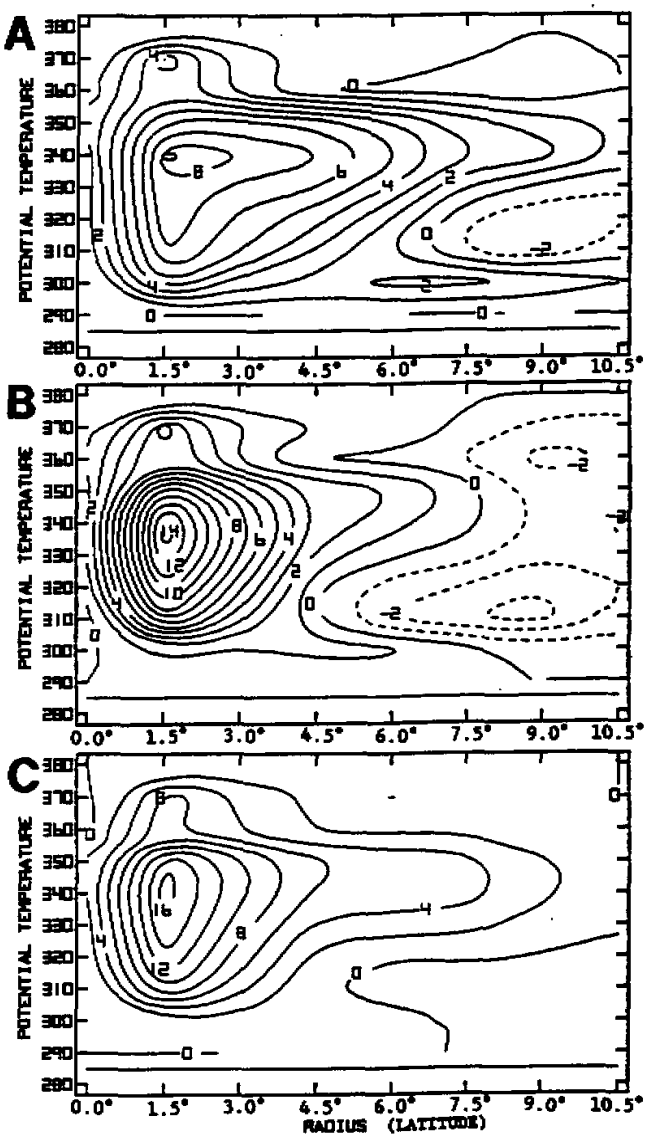

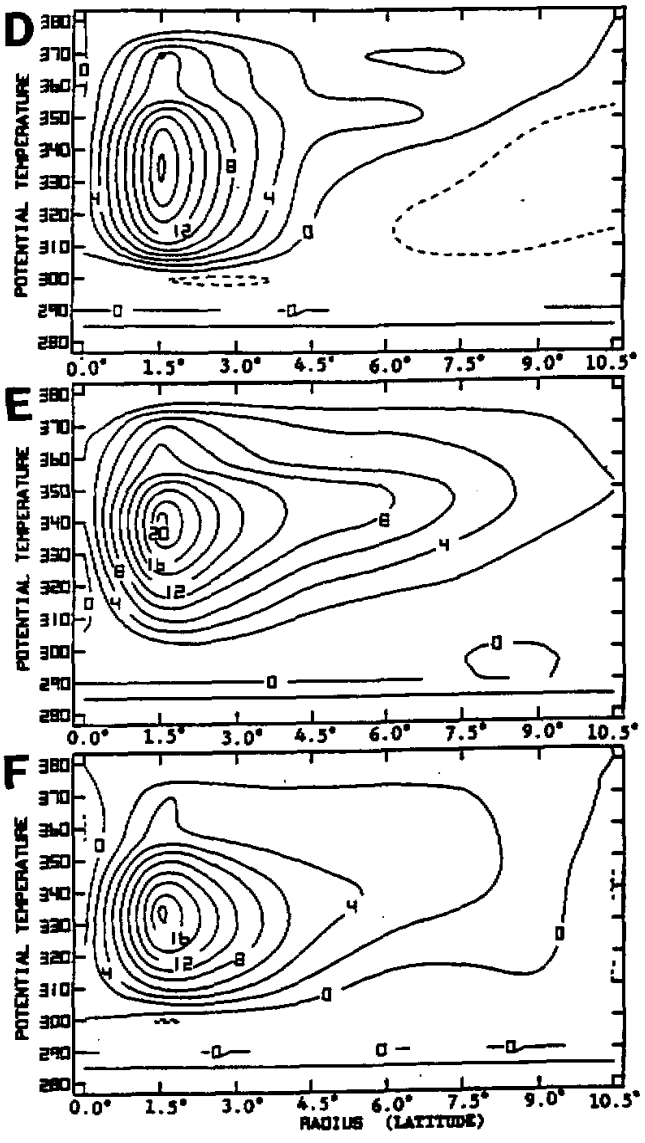

Fig. 21. The vertical–radial distribution of azimuthally–averaged mass–weighted diabatic heating (K day^{-1}) for typhoon Nancy. (a) 0000–1200 UTC 18, (b) 1200 UTC 18–0000 UTC 19, (c) 0000–1200 UTC 19, (d) 1200 UTC 19–0000 UTC 20, (e) 0000–1200 UTC 20 and (f) 1200 UTC 20–0000 UTC 21 September 1979.

(i) *The effect of diabatic heating*

The presence of high SST and the cross–equatorial current throughout the life cycle of Nancy implies that sufficient moisture is available to maintain the typhoon during that time

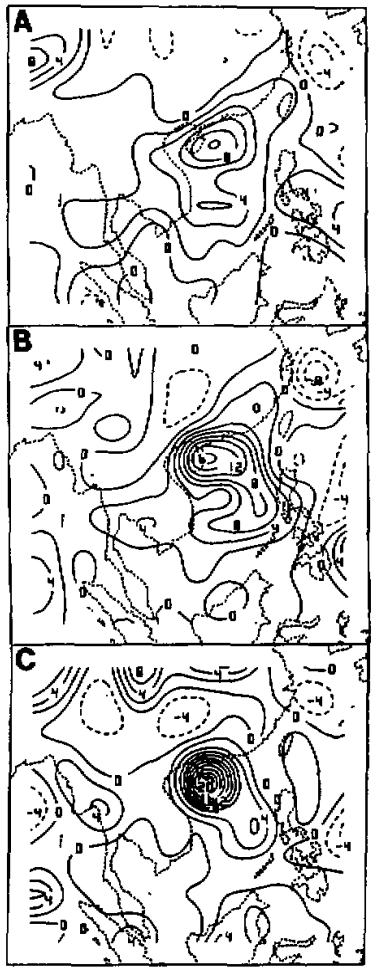

Fig. 22. Horizontal distribution of vertically averaged diabatic heating (K day^{-1}) for typhoon Nancy. (a) 1200 UTC 18, (b) 1200 UTC 19 and (c) 0000 UTC 20 September 1979.

period. Figures 21a and 22a indicate that before the formation of typhoon Nancy, the latent heating rate within the system has already reached 8 K day^{-1}. Latent heat release increases to 20°K day^{-1} from 0000 UTC 18 to 0000 UTC 20 September and becomes concentrated at small radii within a relatively axisymmetric distribution (Figs. 21, 22). The strong heating rate and associated upward diabatic mass transport are coupled with strong inflow in the lower valued isentropic layers and outflow in the higher valued isentropic layers (Figs. 23c–f). The diabatic heating decreases after 1200 UTC 21 when typhoon Nancy moves away from the South China Sea towards Vietnam (Yuan, 1994).

In contrast with the effect of diabatic heating on the Ohio cyclone, the effect of heating on typhoon Nancy leads to relatively strong radial motions with inflow in lower valued isentropic layers and outflow in higher valued isentropic layers (Figs. 23, 10d). This difference

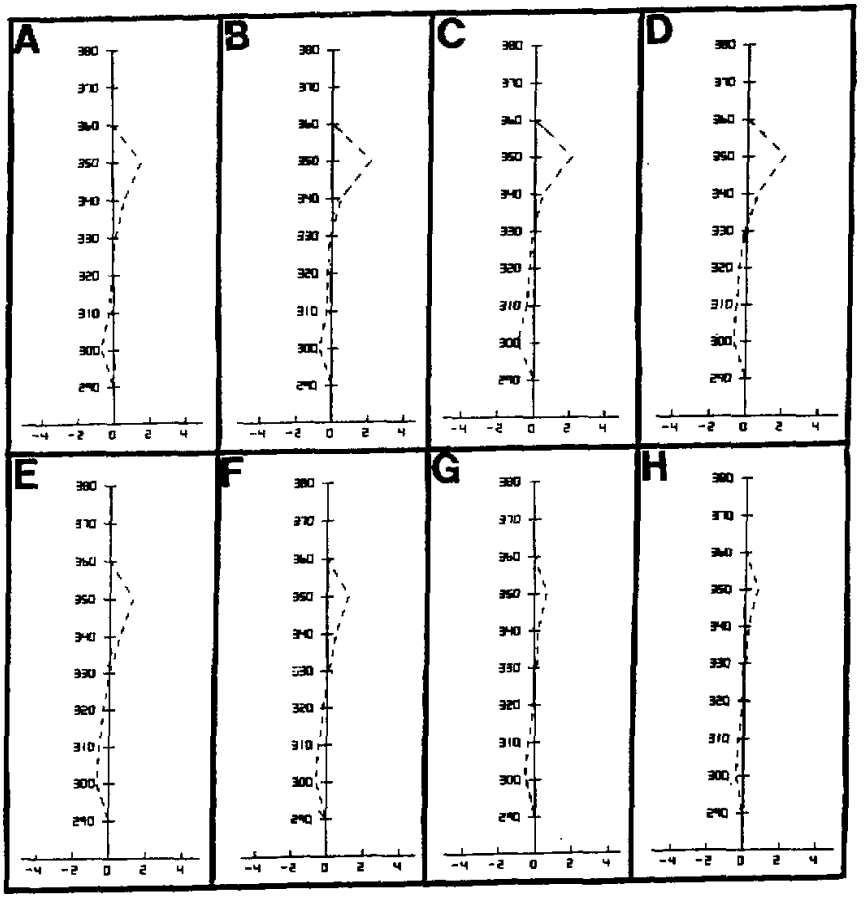

Fig. 23. Vertical profiles of simulated azimuthally-averaged mass-weighted radial motion (m s^{-1} outflow positive) forced by diabatic heating for the radius of 6.0° within typhoon Nancy at (a) 1200 UTC 18, (b) 0000 UTC 19, (c) 1200 UTC 19, (d) 0000 UTC 20, (e) 1200 UTC 20, (f) 0000 UTC 21, (g) 1200 UTC 21 and (h) 0000 UTC 22, September 1979.

likely results from the condition that the dominant order of hydrodynamic stability, represented by

$$\delta^2 = AC - B^2 \tag{14}$$

is one order of magnitude smaller for typhoon Nancy than for the Ohio cyclone. According to Eliassen (1951), for given forcing the radial-vertical circulation intensifies as hydrodynamic stability decreases.

(ii) *The effect of the horizontal and vertical eddy modes*

In their study of the effect of horizontal eddy fluxes of angular momentum on hurricanes, Challa and Pfeffer (1980) point out that the nonlinear effects of asymmetric structure of environment prior to the formation of hurricanes are associated with the eddy angular momentum transport. Their model which includes the horizontal convergence of eddy angular mo-

mentum transport initiates a hurricane whereas purely symmetric models do not. The present study shows that the effect of horizontal eddy mode on the radial motion within typhoon Nancy is likely important in the early stage of the development due to the asymmetric structure of the environment within the ITCZ, as well as the easterly wave (Figs. 102, 103 in Yuan, 1994).

The maximum effect of vertical eddy angular momentum transport on the radial motion within typhoon Nancy occurred during the first time period in this study. Still this effect is smaller than that of horizontal eddy angular momentum transport (Figs. 104, 105 in Yuan, 1994), which is partly due to the fact that diabatic heating is quite symmetric around the low system (Fig. 22).

(iii) *The effect of pressure, inertial and frictional torques*

Within a tropical air mass with weak baroclinity in the lower troposphere, a relatively weak effect of pressure torque is expected on the forcing of the radial motion for the radius of 6.0° within typhoon Nancy (Figs. 106, 107 in Yuan, 1994). This study shows that the forcing associated with pressure torque with a maximum order of magnitude of 10^{-13} (the same order as other terms) occurs only in a thin layer in the early stage. With the intensification of Nancy and development of symmetry, the order of magnitude of pressure torque decreases.

Since the forcing associated with inertial torque with a maximum order of magnitude of 10^{-13} only appears in a thin layer where hydrodynamic stability is relatively strong, this term is not as important as the diabatic forcing except at 0000 UTC 20 September (Fig. 24). At 0000 UTC 20 the horizontal convergence becomes stronger in the region to the south of Hainan Island (Figs. 87d, e, f in Yuan, 1994). This convergence leads to an increase of hydrostatic mass in the southern portion of the storm volume (Fig. 25). Since the typhoon moves southwestward towards the maximum center of hydrostatic mass at this time, the

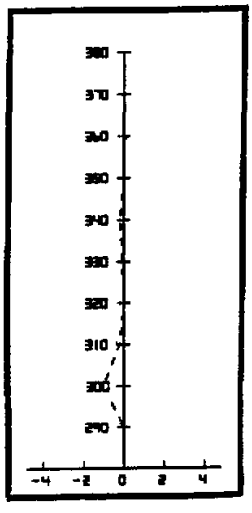

Fig. 24. Vertical profile of simulated azimuthally-averaged mass-weighted radial motion (m s^{-1} outflow positive) forced by inertial torque for the radius of 6.0° within typhoon Nancy at 0000 UTC 20 September 1979.

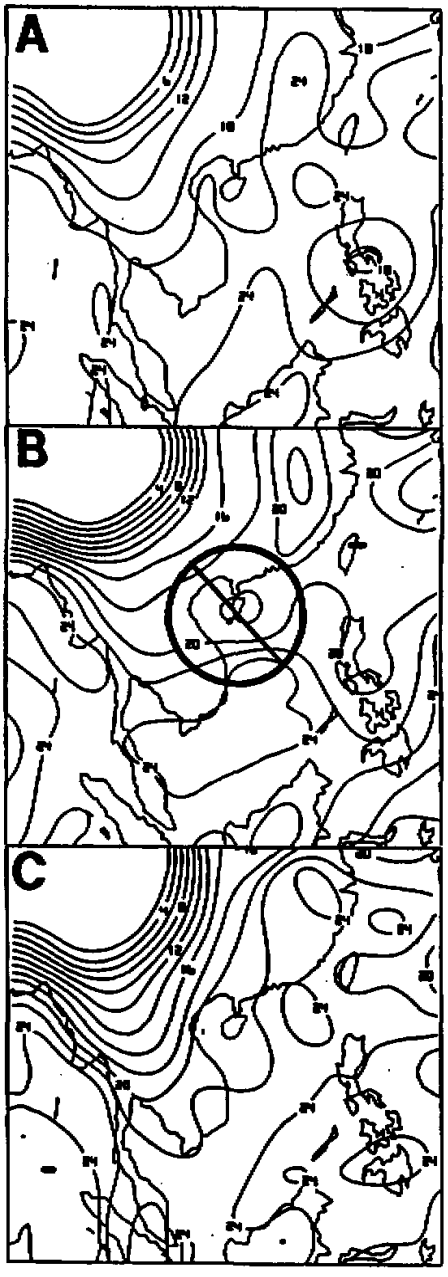

Fig. 25. Hydrostatic mass distribution (10 kg m^{-2}) for typhoon Nancy on 300 K at (a) 1200 UTC 19, (b) 0000 UTC 20 and (c) 1200 UTC 20 September 1979. The circle with the radius equivalent to 6.0° latitudinal arc represents the position of the quasi-Lagrangian storm volume.

storm's relative motion carries more hydrostatic mass into the storm volume in the leading half of the volume than out in the trailing half of the storm volume.

In assessing the relative importance of frictional torque, the drag coefficient of 0.9×10^{-3} is selected based on the results of Garratt (1977). This study shows that a relatively larger contribution of frictional torque to the forced radial motion occurs during the period of time when typhoon Nancy is over Hainan Island than during the time when the system is over the South China Sea (Figs. 111, 112 in Yuan, 1994).

(4) *Summary*

The effect of asymmetric structure of the environment on the forcing of the azimuthally-averaged circulation within typhoon Nancy is mainly represented by the horizontal eddy mode. The positive horizontal eddy mode is likely important in the early stage of development due to the existence of asymmetry associated with ITCZ, an easterly wave and other tropical distrubances. Through the convergence of eddy and mean angular momentum transport and favorable conditions such as high SST and small vertical horizontal-wind shear, the easterly wave amplifies with the intensification of latent heat release. The results of this study verify that the release of latent heat energy is a crucial internal process for the forcing of the radial-vertical circulation and the development of typhoon Nancy. A quantitative example is given here to display the major effects of internal forcing and outer boundary condition on the maximum total radial motion at 0000 UTC 20 September 1979 (dashed line in Fig. 20d). The contribution of 2.1 m s^{-1} outflow to the maximum total outflow of 4 m s^{-1} (Fig. 20 d) at 350 K is from diabatic forcing (Fig. 23d), 0.8 m s^{-1} outflow from horizontal eddy mode (Fig. 102d in Yuan, 1994) and 0.6 m s^{-1} outflow from outer boundary effect which is the homogeneous solution of (1) with open outer boundary conditions.

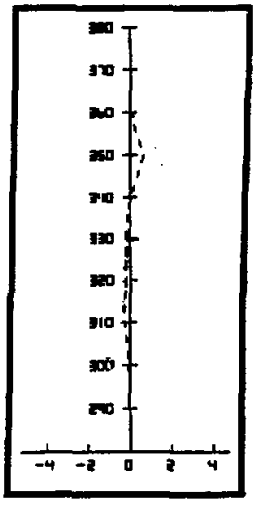

Fig. 26. Vertical profile of azimuthally-averaged mass-weighted radial motion (m s^{-1} outflow positive) obtained from the homogeneous solution of the linear equation with open boundary condition for the radius of 6.0° within typhoon Nancy at 0000 UTC 20 September 1979.

Another important factor affecting the intensity of the radial–vertical circulation within typhoon Nancy is the weak hydrodynamic stability of the environment. The dominant magnitude of hydrodynamic stability for typhoon Nancy is one order of magnitude smaller than those for the Ohio cyclone.

The conclusion from this isentropic numerical study of typhoon Nancy is in agreement with the theoretical conclusions drawn by Charney and Eliassen (1964) for the development of a tropical cyclone. In their conclusions, diabatic heating and forced inflow are important factors. The forced inflow within the planetary boundary layer (PBL) carries moist static energy and angular momentum into the convection within the eyewall. Furthermore, sensible and latent energy fluxes from the warm ocean to the system occur as the air within the PBL moves horizontally towards lower pressure and cools through dry adiabatic expansion. The resulting static instability in the PBL in conjunction with turbulence leads to marked increases of moist static energy and the high equivalent potential temperature needed for maintenance of deep convection with the eyewall. The perspective set forth recently by Emanuel et al. (1994) and Emanuel (1996) which calls attention to the importance of spatial and temporal distribution of the subcloud–layer entropy in relation to the large–scale circulation within tropical cyclones and their environment is in accord with the earlier application of Eliassen's (1951) perspective to the hurricane by Charney and Eliassen (1964). Limited by the spatial and temporal resolutions used in this numerical study as well as in the ECMWF FGGE IIIb data, the present study cannot resolve the moist convective processes within the eyewall emphasized by Emanuel and co–authors.

V. SUMMARY AND CONCLUSIONS

A concept of the zonally averaged general circulation in isentropic coordinates was introduced by Dutton (1976) based on the perspective that hemispheric isentropic meridional circulation was forced by large scale heat sources and sinks. Following the development of the theory for the forcing of the meridional circulation within a stable and symmetric circumpolar vortex (Eliassen, 1951), this concept and approach were used in developing the theory for the forced isentropic meridional circulation within an asymmetric circumpolar vortex (Gallimore and Johnson, 1981). Gallimore and Johnson's work in conjunction with Johnson and Downey's storm relative mass and storm angular momentum budget study facilitated the development of a diagnostic equation for simulating the forced azimuthally–averaged mass–weighted radial–vertical circulation within translating extratropical and tropical cyclones (Johnson and Yuan, 1998a). The forcing in this equation includes pressure torque (representing the baroclinic structure of atmosphere) and inertial torque (representing net transport of mass due to the movement of storm volume in an environment with asymmetric mass distribution). In addition to these two torques which are implicit in isobaric studies, this isentropic study also includes the effects of eddy angular momentum transport, diabatic heating, frictional torque and the trade off between the forcing and hydrodynamic stability (static, inertial and baroclinic stability), which are included in isobaric studies. Since the equation is linear and diagnostic, this study does not resolve the evolution of radial motion in terms of nonlinearity and feedback between the various processes.

With the use of the linear diagnostic equation, the total and individual components of azimuthally–averaged mass–weighted radial motion within cyclones have been simulated to ascertain the relative importance of the stability and internal physical processes responsible for forcing the radial motion in relation to cyclone development, maintenance and decay.

The two cyclones selected for this study were the Ohio extratropical cyclone of 25–27 January 1978 and typhoon Nancy of 18–23 September 1979. In a previous mass and angular momentum budget study of the Ohio cyclone utilizing quasi–Lagrangian diagnostics, Hale (1983) showed that the mean radial–vertical mass circulation with convergence of mass in the lower valued isentropic layers and divergence in the higher valued isentropic layers was the most intense within the Ohio cyclone relative to other cyclones. The strong inward transport of angular momentum by the mass circulation induced low–level rotation and an S–shaped deformation of low–level thermal field with the concurrent adjustment of upper–level flow through the thermal wind. As a part of the self–development process (Sutcliffe, 1947; Palmen and Newton, 1969; Johnson and Hill, 1987), the S–shaped upper–level wind pattern favored a strong eddy angular momentum convergence. This self–development process combined with the upward diabatic angular momentum transport due to intense latent heat release and the angular momentum transfer due to pressure stresses contributed to the spin up throughout the troposphere. The present numerical simulations show that within the Ohio extratropical cyclone, the dominant internal physical processes for forcing the radial motion which is responsible for the net inward transport of angular momentum needed for the development are: 1) pressure torque that is uniquely related to the geostrophic wind distribution within the baroclinic structure of the vortex and its environment and 2) the horizontal eddy angular momentum transport that is related to the advection of vorticity. The diabatic heating is mainly responsible for forcing the vertical branch of the radial–vertical circulation in isentropic coordinates.

Different from the extratropical Ohio cyclone, the development and maintenance of typhoon Nancy can be explained by the CISK mechanism (Charney and Eliassen, 1964). In the CISK theory, Charney and Eliassen demonstrate the importance of the interaction between deep convection within the eyewall and the forced inflow within the PBL in supplying the tropical cyclone with moist static energy and angular momentum. Their theory is verified by this study of typhoon Nancy. Before the formation of typhoon Nancy, the latent heat release within an easterly wave had already induced a radial–vertical circulation with inward angular momentum transport in lower valued isentropic layers. In addition, inward eddy angular momentum transport (associated with the asymmetric structure of the environment due to the ITCZ, the easterly wave and an upper–layer weak anticyclone) combined with high SST and weak vertical shear of horizontal wind also favored the development of the system. The increase of angular momentum and water vapor within the system due to the net import through the radial–vertical circulation with inflow in lower valued isentropic layers and outflow in higher valued isentropic layers led to the development of typhoon Nancy. The numerical simulations show that the intensification of this forced radial–vertical circulation within typhoon Nancy is mainly associated with diabatic forcing and weak hydrodynamic stability.

The present results show that the simulated radial motions within the two cyclones agree quite well with observed radial motions. The excellent agreement verifies the applicability of Eliassen's perspective to study the forcing of the radial–vertical circulations within extratropical and tropical cyclones. This study also demonstrates the capability of the linear diagnostic equation to assess the relative importance of internal physical processes in forcing the azimuthally–averaged mass–weighted radial–vertical circulation within translating extratropical and tropical cyclones.

Table 1. The Ranges of the Order of Magnitude of Hydrodynamic Stability and the Maximum Order of Magnitude of the Forcing Terms for the Ohio Storm for the 7.5° Radius

time	stability	term $1^{(1)}$	term $2^{(2)}$	term $3^{(3)}$	term $4^{(4)}$	term $5^{(5)}$	term $6^{(6)}$	term $7^{(7)}$
25^{12}	$10^{-11\sim-13}$	10^{-11}	10^{-12}	10^{-12}	10^{-11}	10^{-12}	10^{-12}	10^{-13}
26^{00}	$10^{-11\sim-12}$	10^{-11}	10^{-12}	10^{-12}	10^{-11}	10^{-11}	10^{-12}	10^{-12}
26^{12}	$10^{-11\sim-12}$	10^{-11}	10^{-12}	10^{-11}	10^{-11}	10^{-11}	10^{-12}	10^{-11}
27^{00}	$10^{-11\sim-12}$	10^{-11}	10^{-12}	10^{-11}	10^{-11}	10^{-11}	10^{-12}	10^{-11}

Table 2. The Ranges of the Order of Magnitude of Hydrodynamic Stability and the Maximum Order of Magnitude of the Forcing Terms for the Typhoon Nancy for the 6.0° Radius

time	stability	term $1^{(1)}$	term $2^{(2)}$	term $3^{(3)}$	term $4^{(4)}$	term $5^{(5)}$	term $6^{(6)}$	term $7^{(7)}$
18^{12}	$10^{-12\sim-13}$	10^{-13}	10^{-13}	10^{-13}	10^{-13}	10^{-13}	10^{-14}	10^{-14}
19^{00}	$10^{-12\sim-13}$	10^{-14}	10^{-13}	10^{-14}	10^{-13}	10^{-13}	10^{-14}	10^{-13}
19^{12}	$10^{-12\sim-13}$	10^{-13}	10^{-13}	10^{-13}	10^{-13}	10^{-13}	10^{-14}	10^{-14}
20^{00}	10^{-13}	10^{-14}	10^{-13}	10^{-13}	10^{-13}	10^{-13}	10^{-14}	10^{-13}
20^{12}	10^{-13}	10^{-14}	10^{-13}	10^{-13}	10^{-13}	10^{-13}	10^{-14}	10^{-13}
21^{00}	$10^{-12\sim-13}$	10^{-14}	10^{-13}	10^{-13}	10^{-13}	10^{-13}	10^{-14}	10^{-13}
21^{12}	$10^{-12\sim-13}$	10^{-14}	10^{-13}	10^{-14}	10^{-13}	10^{-13}	10^{-14}	10^{-13}
22^{00}	$10^{-12\sim-13}$	10^{-14}	10^{-13}	10^{-14}	10^{-13}	10^{-14}	10^{-14}	10^{-13}

The unit of stability is m^2s^{-4} hPa^{-2} and the unit of all the forcing term is m s^{-3} hPa^{-1}. The forcing terms associated with: [1]pressure torque; [2]horizontal variation of azimuthally-averaged mass-weighted diabatic heating; [3]divergence of vertical eddy angular momentum transport; [4]divergence of horizontal eddy angular momentum transport; [5]inertial torque; [6]tilting of angular momentum towards or away from the local vertical axis due to cyclone's movement over the spherical earth; [7]frictional torque

The authors would like to thank Mr. Todd Schaack and Professor Kim Van Scoy for their scientific and editorial contributions.

Appendix A

The Diagnostic Equation for the Radial-Vertical Circulation within Cyclones and Its Difference Scheme

According Dutton (1976), an isentropic meridional circulation is directly forced by heat sources / sinks and torques. In the representation of the physical processes as they relate to the forced azimuthally-averaged mass-weighted radial-vertical circulation, the diagnostic equation (1) is now transformed from the azimuthally-averaged mass coordinates $(\Phi(\beta),\bar{p}(\beta,\theta,t),t)$ with $\bar{p}(\beta,\theta,t)=g\bar{m}(\beta,\theta,t)=g\int_{\theta}^{\theta_T}\overline{\rho J_\theta}\,d\theta$ back to isentropic coordinates (β,θ,t). This transformation is based on the following relations (Gallimore and Johnson, 1981; Yuan, 1990)

$$\frac{\partial}{\partial\Phi_p}=\frac{1}{a}\frac{\partial}{\partial\beta_\theta}-\frac{1}{a}\frac{\partial\bar{p}}{\partial\beta_\theta}\frac{\partial}{\partial\bar{p}}$$

$$= \frac{\partial}{\partial \Phi_\theta} - \frac{\partial \bar{p}}{\partial \Phi_\theta}\frac{\partial}{\partial \bar{p}} \tag{A.1}$$

$$\frac{\partial()}{\partial \bar{p}} = \frac{1}{\partial \bar{p} / \partial \theta}\frac{\partial()}{\partial \theta}. \tag{A.2}$$

First, a flux form of (1) in (β,θ,t) coordinates will be derived. For clarity of the derivation, let M and N represent the sum of terms in the first and second parentheses on the left hand side of (1) respectively, that is

$$M = A\frac{\partial S}{\partial \Phi_p} + B\frac{\partial S}{\partial \bar{p}} \tag{A.3}$$

and

$$N = B\frac{\partial S}{\partial \Phi_p} + C\frac{\partial S}{\partial \bar{p}}. \tag{A.4}$$

With the use of (A.1), (A.2) and the definition of M and N, (1) is rewritten as

$$\frac{\partial M}{\partial \Phi_\theta} - \frac{\partial \bar{p}}{\partial \Phi_\theta}\frac{1}{\partial \bar{p} / \partial \theta}\frac{\partial M}{\partial \theta} + \frac{1}{\partial \bar{p} / \partial \theta}\frac{\partial N}{\partial \theta} = \text{forcing terms.} \tag{A.5}$$

The multiplication of (A.5) by $(\partial \bar{p} / \partial \theta)$ yields

$$\begin{aligned}
&\frac{\partial \bar{p}}{\partial \theta}\frac{\partial M}{\partial \Phi_\theta} - \frac{\partial \bar{p}}{\partial \Phi_\theta}\frac{\partial M}{\partial \theta} + \frac{\partial N}{\partial \theta} \\
&= \frac{\partial}{\partial \Phi_\theta}(M\frac{\partial \bar{p}}{\partial \theta}) - M\frac{\partial^2 \bar{p}}{\partial \Phi_\theta \partial \theta} - \frac{\partial}{\partial \theta}(M\frac{\partial \bar{p}}{\partial \Phi_\theta}) + M\frac{\partial^2 \bar{p}}{\partial \Phi_\theta \partial \theta} + \frac{\partial N}{\partial \theta} \\
&= \frac{\partial}{\partial \Phi_\theta}(M\frac{\partial \bar{p}}{\partial \theta}) - \frac{\partial}{\partial \theta}(M\frac{\partial \bar{p}}{\partial \Phi_\theta}) + \frac{\partial N}{\partial \theta} \\
&= \text{forcing terms } x(\partial \bar{p} / \partial \theta).
\end{aligned} \tag{A.6}$$

At this point, (A.6) is in a flux form. With M and N [see (A.3) and (A.4)] transformed into (β,θ,t) coordinates

$$\begin{aligned}
M &= A(\frac{\partial S}{\partial \Phi_\theta} - \frac{\partial \bar{p}}{\partial \Phi_\theta}\frac{1}{\partial \bar{p} / \partial \theta}\frac{\partial S}{\partial \theta}) + B\frac{1}{\partial \bar{p} / \partial \theta}\frac{\partial S}{\partial \theta} \\
&= A\frac{\partial S}{\partial \Phi_\theta} + \frac{1}{\partial \bar{p} / \partial \theta}(-A\frac{\partial \bar{p}}{\partial \Phi_\theta} + B)\frac{\partial S}{\partial \theta}
\end{aligned} \tag{A.7}$$

and

$$N = B\frac{\partial S}{\partial \Phi_\theta} + \frac{1}{\partial \bar{p} / \partial \theta}(-B\frac{\partial \bar{p}}{\partial \Phi_\theta} + C)\frac{\partial S}{\partial \theta}, \tag{A.8}$$

the substitution of (A.7) and (A.8) into (A.6) yields the final flux form of the diagnostic equation expressed in (β,θ,t) coordinates.

$$\begin{aligned}
&\frac{\partial}{\partial \Phi_\theta}[A\frac{\partial S}{\partial \Phi_\theta}\frac{\partial \bar{p}}{\partial \theta} + (-A\frac{\partial \bar{p}}{\partial \Phi_\theta} + B)\frac{\partial S}{\partial \theta}] - \frac{\partial}{\partial \theta}[A\frac{\partial S}{\partial \Phi_\theta}\frac{\partial \bar{p}}{\partial \Phi_\theta} + \frac{1}{\partial \bar{p} / \partial \theta}\frac{\partial \bar{p}}{\partial \Phi_\theta}(-A\frac{\partial \bar{p}}{\partial \Phi_\theta} \\
&\quad + B)\frac{\partial S}{\partial \theta}] \\
&+ \frac{\partial}{\partial \theta}[B\frac{\partial S}{\partial \Phi_\theta} + \frac{1}{\partial \bar{p} / \partial \theta}(-B\frac{\partial \bar{p}}{\partial \Phi_\theta} + C)\frac{\partial S}{\partial \theta}]
\end{aligned}$$

$$= \text{forcing terms } x(\partial\bar{p}/\partial\theta). \tag{A.9}$$

The finite difference equation which approximates the diagnostic (A.9) is obtained by applying the second-order centered difference to both horizontal and vertical derivatives. To solve the finite difference equation, the successive-over-relaxation (SOR) iteration method was utilized (Yuan, 1994) with over relaxation factor $\omega^* = 1.8$ (Strikwerda, 1989).

Appendix B

The Calculation of Coefficients and Forcing Components

The purpose of this appendix is to present the methods for numerically representing the coefficients on the left of (1) that are determined by the state structure and also the forcing terms on the right of (1) that deal with physical processes.

1. *The calculation of coefficients*

Coefficients A, B and *C* in (1) represented by $(\bar{\Phi},p)$ coordinates will be rewritten in (β,θ) coordinates as

$$A = -\frac{\alpha_*}{\sin\beta}\left(\frac{\partial\bar{p}}{\partial\theta}\right)^{-1} \tag{B.1}$$

$$\begin{aligned} B &= \frac{\alpha_*}{\sin\beta}\frac{\partial\theta}{\partial\bar{\Phi}_{\bar{p}}} \\ &= \frac{\alpha_*}{\sin\beta}\left(\frac{1}{a}\frac{\partial\theta}{\partial\beta_\theta} - \frac{1}{a}\frac{\partial\bar{p}}{\partial\beta_\theta}\frac{\partial\theta}{\partial\bar{p}}\right) \\ &= -\frac{\alpha_*}{\sin\beta}\frac{\partial\bar{p}}{\partial\Phi_\theta}\left(\frac{\partial\bar{p}}{\partial\theta}\right)^{-1} \end{aligned} \tag{B.2}$$

$$\begin{aligned} C &= \frac{1}{a^3\sin^4\beta}\frac{\hat{c}}{\partial\Phi_{\bar{p}}}(g_{az}{}^2) \\ &= \frac{1}{a^3\sin^4\beta}\left[\frac{\partial(g_{az}{}^2)}{\partial\Phi_\theta} - \frac{\partial\bar{p}}{\partial\Phi_\theta}\frac{\partial(g_{az}{}^2)}{\partial\theta}\left(\frac{\partial\bar{p}}{\partial\theta}\right)^{-1}\right]. \end{aligned} \tag{B.3}$$

Based on centered differencing, the following schemes are used for calculating coefficients *A*, *B* and *C* at grid points

$$A_{i,j} = -\frac{\alpha_*}{\sin\beta}\left(\frac{\bar{p}_{i+1,j} - \bar{p}_{i-1,j}}{2\Delta\theta}\right)^{-1} \tag{B.4}$$

$$B_{i,j} = -\frac{\alpha_*}{\sin\beta}\left(\frac{\bar{p}_{i,j+1} - \bar{p}_{i,j-1}}{2\Delta\Phi_\theta}\right)\left(\frac{\bar{p}_{i+1,j} - \bar{p}_{i-1,j}}{2\Delta\theta}\right)^{-1} \tag{B.5}$$

$$\begin{aligned} C_{i,j} = &\frac{1}{a^3\sin^4\beta}\left[\frac{(g_{az}{}^2)_{i,j+1} - (g_{az}{}^2)_{i,j-1}}{2\Delta\Phi_\theta}\right] \\ &- \frac{\bar{p}_{i,j+1} - \bar{p}_{i,j-1}}{2\Delta\Phi_\theta}\frac{(g_{az}{}^2)_{i+1,j} - (g_{az}{}^2)_{i-1,j}}{2\Delta\theta}\left(\frac{\bar{p}_{i+1,j} - \bar{p}_{i-1,j}}{2\Delta\theta}\right)^{-1}. \end{aligned} \tag{B.6}$$

and at half points of the grid (e.g. $A_{i+1/2,j}$, $B_{i+1/2,j}$ and $C_{i+1/2,j}$)

$$A_{i+1/2,j} = -\frac{\alpha_*}{\sin\beta}\left(\frac{\bar{p}_{i+1,j} - \bar{p}_{i,j}}{\Delta\theta}\right)^{-1} \tag{B.7}$$

$$B_{i+1/2,j} = -\frac{\alpha_*}{\sin\beta}\left(\frac{\bar{p}_{i+1/2,j+1}-\bar{p}_{i+1/2,j-1}}{2\Delta\Phi_\theta}\right)\left(\frac{\bar{p}_{i+1,j}-\bar{p}_{i,j}}{\Delta\theta}\right)^{-1} \tag{B.8}$$

$$C_{i-1/2,j} = \frac{1}{a^3\sin^4\beta}\left[\frac{(g_{az}{}^2)_{i+1/2,j+1}-(g_{az}{}^2)_{i+1/2,j-1}}{2\Delta\Phi_\theta} - \frac{\bar{p}_{i+1/2,j+1}-\bar{p}_{i+1/2,j-1}}{2\Delta\Phi_\theta}\,\frac{(g_{az}{}^2)_{i+1,j}-(g_{az}{}^2)_{i,j}}{\Delta\theta}\left(\frac{\bar{p}_{i+1,j}-\bar{p}_{i,j}}{2\Delta\theta}\right)^{-1}\right]. \tag{B.9}$$

Finite differencing of the second-order differentiation of pressure with respect to the radius limits the evaluation of streamfunction S to the interior four of eight radii. Therefore, a cubic spline method is applied in order to calculate the horizontal pressure gradient on isentropic surfaces for all eight radii. The finite differencing schemes for the calculation of pressure torque, frictional torque, the vertical and horizontal divergences of eddy angular momentum transport [see (4)] are presented in the following section.

2. The calculation of forcing components

(1) *Pressure torque*

By definition, the pressure torque as product of pressure gradient force and the distance from the storm center is represnted by

$$-\frac{\partial\psi}{a\sin\beta\partial\alpha_\theta}a\sin\beta = -\frac{\partial\psi}{\partial x_\theta}. \tag{B.10}$$

Applying a centered difference to right of (B.10) yields

$$-\frac{\partial\psi}{\partial\alpha_\theta} = -\frac{\psi_{m+1}-\psi_{m-1}}{2\Delta\alpha}.$$

Since α representing the azimuthal direction is from zero to 2π, the calculation of the pressure torque does not involve boundary conditions.

(2) *Frictional torque*

With hydrostatic balance and the assumption that the frictional stress at the top of the planetary boundary layer (PBL) τ_{top} is zero (after Lettau 1959), the frictional torque in (4) is represented by

$$\begin{aligned}\vec{\Gamma}\cdot\vec{F}a\sin\beta &= a\sin\beta\vec{\Gamma}\cdot\frac{1}{\rho J_\theta}\frac{\partial\vec{\tau}}{\partial\theta}\\ &\cong \frac{a\sin\beta}{-(\Delta p/\Delta\theta)/g}\vec{\Gamma}\cdot\frac{\vec{\tau}_{top}-\vec{\tau}_{sfc}}{\Delta\theta}\\ &= \frac{1}{\Delta p/g}(\vec{\tau}\cdot\vec{\Gamma}a\sin\beta)_{sfc},\end{aligned} \tag{B.11}$$

where Δp equals the pressure at the bottom minus the pressure at the top of PBL. The frictional stress at the bottom of this boundary layer is defined as (after Lettau, 1959)

$$\vec{\tau}_{sfc} = \rho C_g{}^2|\vec{U}_{sfc}|\vec{U}_{sfc}, \tag{B.12}$$

where the surface wind is replaced by geostrophic wind. The assigned angle between geostrophic wind and the azimuthal direction is 45°; the value used in the previous mass and angular momentum budget study of cyclones (Hale, 1983; Katzfey, 1978; Johnson and Hill,

1986). The values of the drag coefficient $C_g{}^2$ which range from 0.03^2 to 0.083^2 were adjusted to obtain the most suitable simulated profiles in relation to the "observed" profiles of radial motion within cyclones selected for case study. $C_g{}^2$ equal to 0.03^2 is the minimum of $C_g{}^2$ over the sea (Garratt, 1977). Equation (B.11) states that the frictional torque within PBL is proportional to the frictional stress at the earth's surface divided by the mass $(\Delta p / g)$ in lowest isentropic layer. If Δp in the lowest isentropic layer is less than 100 hPa, then the mass in the lowest two layers is combined and then given to Δp.

(3) *Horizontal divergence of eddy angular momentum transport*

The radial and vertical divergences of eddy angular momentum [term 7 and term 8 in (4)] are calculated based on a centered difference scheme. Since this is a diagnostic study, the data for calculating the transport of g_{az}, $(u- w)_\beta$ and $\dot{\theta}$, are available at every grid point. $\dot{\theta}$ is obtained through the use of the mass continuity equation in isentropic coordinates.

Appendix C

List of Symbols

Symbol

a	radius of earth
c_p	specific heat at constant pressure
f	Coriolis parameter at latitude φ
f_0	Coriolis parameter at latitude φ_0
$\tilde{f}$	$0.5(f+ f_0)$
g	acceleration due to gravity
g_{az}	vertical component of absolute angular momentum
h	height of isentropic surface
k_n	azimuthal wavenumber
m	mass
p	pressure
$\bar{p}$	$\int_{\theta_r}^{\theta} \frac{\partial \bar{p}}{\partial \theta} d\theta$
P_{00}	1000 hPa
S	streamfunction
t	time
z	height above sea level
$\hat{F}$	sum of torques
J_θ	Jacobian for transformation, $\lvert \partial z / \partial \theta \rvert$
K	Kelvin
R	gas constant for dry air
R_β	$-(a\sin\beta)^3$
T	temperature
Δp	amplitude of azimuthal wave
α	azimuthal coordinate
α_*	$(R / \bar{p})(\bar{p} / p_{00})^\kappa$
β	radial coordinate defined by angular distance
θ	potential temperature
ψ	Montgomery streamfunction

κ	R / c_p
ρ	density
φ	latitude
φ_0	latitude of the center of a storm
Φ	radial coordinate in $(\Phi,\bar{p})$ coordinates defined by length
ω_p	$d\bar{p} / dt$

Subscripts and Superscripts

a	absolute frame of reference
B	bottom or boundary
o	budget volume central reference axis
$\bar{p}$	$\bar{p}$ coordinate
s	surface of the earth
T	top of atmosphere
z	vertical direction
α	azimuthal component
β	radial component
θ	isentropic coordinate system; isentropic surface

Vectors

$\vec{F}$	frictional force
$\vec{U}$	earth–relative wind velocity
$\vec{W}$	earth–relative velocity of lateral boundary
$\vec{g}_a$	absolute angular momentum
$\vec{m}$	unit vector in radial direction
$\vec{l}$	unit vector in azimuthal direction
$\vec{k}$	unit vector in vertical direction
$\vec{r}$	position vector
$\vec{\Omega}$	angular velocity of the earth

Operators

$\frac{\partial}{\partial\theta}$	partial derivative with respect to θ
$\frac{\delta}{\delta t_\theta}$	quasi–Lagrangian time derivative in isentropic coordinates
$\frac{\partial}{\partial\Phi}$	$\frac{1}{a}\frac{\partial}{\partial\beta_{\bar{p}}}$
$\cdot$	$\frac{d}{dt}$
$-$	azimuthal average
$\wedge,< >$	mass–weighted azimuthal average
$*$	deviation from mass–weighted azimuthal average
$'$	deviation from azimuthal average
∇	horizontal del operator
$\int$	Riemann integral
$\lvert\ \rvert$	absolute value

REFERENCES

Adrian, B. (1981), *The mass and angular momentum budgets of a developing over the East China Sea*, M. S. thesis,

University of Wisconsin Madison, 97 pp.

Anthes, R.A. and D. Keyser (1979), Test of a fine–mesh model over Europe and the United States, *Mon. Wea. Rev.*, **107:** 963–984.

Anthes, R.A. and D.R. Johnson (1968), The generation of available potential energy in hurricane Hilda (1964), *Mon. Wea. Rev.*, **96:** 291–305; also in Studies of Large Scale Energetics, Annual Rep. (1967), ESSA Grant 52, Dept. of Meteor., University of Wisconsin–Madison, [NTIS PB–180870], 37–70.

Barnes (1973), Mesoscale objective map analysis using weighted time–series observations *NOAA Tech. Memo ERL NSSL–62*, Norman, OK 60pp.

Burrows, W.R., R.A. Treidl and R.G. Lawford (1979), The southern Ontario blizzard of January 26 and 27, 1978, *Atmo.–Ocean*, **50:** 2038–2053.

Challa, M. and R.L. Pfeffere (1980), Effects of eddy fluxes of angular momentum on model hurricane development, *J. Atmos. Sci.*, **37:** 1603– 1618.

Charney and Eliassen (1964), On the growth of the hurricane depression, *J. Atmos. Sci.*, **21:** 68–75.

Dunn, G.E. and B.I. Miller (1964), Atlantic hurricanes, Louisiana State University Press, Baton Rouge.

Dutton, J.A. (1976), The Ceaseless Wind, McGraw–Hill, 579 pp.

Edman, A.D. (1979), *A comparison of the ageostrophic motion and divergence associated with jet streaks in isentropic and isobaric coordinates*, M.S. thesis, University of Wisconsin, Madison, 39 pp.

Eliassen, A. (1951), Slow thermally or frictionally controlled meridional circulation in a circular vortex, *Astrophysica Norvebica*, **5:** 19–60.

Emanuel, K.A., J.D. Neelin and C.S. Bretherton (1993), On large–scale circulation in convecting atmospheres, *Q.J.R. Meteorol. Soc.*, **120:** 1111–1143.

Emanuel, K.A. (1996), Some aspects of hurricane inner–core dynmaics and energetics, *J. Atmos. Sci.*, **54:** 1014–1026.

Gallimore, R.G. and D.R. Johnson (1981), The forcing of the meridional circulation of the isentropic zonally averaged circumpolar vortex, *J. Atmos. Sci.*, **38:** 583–599.

Garratt, J.R. (1977), Review of drag coefficients over ocean and continents, *Mon. Wea. Rev.*, **105:** 915–929.

Gaza, R.S. and L.F. Bosart (1990), Trough–merger characteristics over North America, *Wea. Forecasting*, **5:** 314–331.

Hakim, G.J., L.F. Bosart and D. Keyser (1995), The Ohio Valley wave–merger cyclogenesis event of 25–26 January 1978, Part I: Multiscale case study, *Mon. Wea. Rev.*, **123:** 2663–2692.

Hakim, G.J., D. Keyser, and L.F. Bosart (1996), The Ohio Valley wave–merger cyclogenesis event of 25–26 January 1978, Part II: Diagosis using quasigeostrophic potential vorticity inversion, *Mon. Wea. Rev.*, **124:** 2176–2205.

Hale, R. (1983), Mass and angular momentum diagnostics of the intense Ohio Valley extratropical cyclone of 25–27 January 1978, M.S. thesis, University of Wisconsin–Madison, 96 pp.

Johnson, D.R. (1974), The absolute angular momentum of cyclones, Subsynoptic Extratropical Weather Sytem: Observations, Analysis, Modeling and Prediction, Volume II seminars and workshops, Colloquium notes of the advanced study program and small–scale analysis and prediction project, National Center for Atmospheric Research, Boulder, CO, [NTIS PB–247286], 821 pp.

——— and W.K. Downey (1975a), Azimuthally averaged transport and budget equations for storms: quasi–Lagrangian diagnostics 1, *Mon. Wea. Rev.*, **103:** 967–979.

——— and ——— (1975b), The absolute angular momentum of storms: quasi–Lagrangian diagnostics 2, *Mon. Wea. Rev.*, **103:** 1063–1077.

——— and ——— (1976), The absolute angular momentum budget of an extratropical cyclone: quasi–Lagrangian diagnostics 3, *Mon. Wea. Rev.*, **104:** 3– 14.

———, C.H. Wash and K.A. Peterson (1976), The mass and absolute angular momentum budgets of the Alerta cyclone of 30 March–2 April 1971, Sixth Conference on Weather Forecasting and Analysis, May 10–13, 1976, Albany, NY. Published by American Meteorological Society, Boston, Massachusetts 02108.

———, ——— and C.H. Wash (1981), The forcing of the extratropical cyclone within an angular momentum perspective (unpublished manuscript).

——— (1981), The extratropical cyclone and its interaction with larger and smaller scales, Seminar presented at New Zealand Meteor. Service, Wellington, New Zealand, November 1981; and Seminar presented at Bureau of Meteor., Melbourne, Australia, November 198.

——— (1988), Extratropical cyclone, angular momentum and nonlinearity, Lecture for the 1988 summer colloquium of the Advanced Study Program of the National Center for Atmospheric Research.

——— (1989), The forcing and maintenance of global monsoonal circulations: An isentropic analysis, Advances in Geophysics, (B. Saltzman, ed.), Academic Press, **31:** 43–316.

——— and D.K. Hill (1987), Quasi-Lagrangian diagnostics of a Mediterranean cyclone: Isentropic results, *Meteorol. Atmos. Phys.*, **36:** 118–140.

——— and Z. Yuan (1998a), On the forcing of the meridional circulation within cyclones, Part I: concepts and equations, *Advances in Atmospheric Sciences*, **15:** 346–369.

Katzfey, J. (1978), A diagnostic of the vertical distribution of angular momentum in isentropic coordinates by pressure torques, M.S. thesis, University of wisconsin Madison, 118 pp.

Kuo, H. L. (1956), Forced and free meridional circulations in the atmosphere, *J. Atmos. Sci.*, **13:** 561–568.

Lattau, H.H. (1959), Wind profile, surface stress and geostrophic drag coefficients in the atmospheric surface layer, *Advances in Geophysics, Academic Press*, **6:** 241–257.

Lorenz, E.N. (1955), Generation of available potential energy and the intensity of the general circulation, In Large scale synoptic processes (J. Bjerknes, proj. dir.), Final Rep., 1957, Contract AF19 (604)–1286 Dept. Meteorol., Univ. of California, Los Angeles.

Malkus, J.S. and H. Riehl (1960), On the dynamics and energy transformations in steady state hurricanes, *Tellus*, **12:** 1–20.

Molinari, M. and D. Vollaro (1990), External influences on hurricane intensity, Part II: Vertical structure and response of the hurricane vortex, *J. Atmos. Sci.*, **47:** 1902–1918.

Molinari, M., D. Vollaro and S. Skubis (1993), Application of the Eliassen balanced model to real-data tropical cyclones, *Mon. Wea. Rev.*, **121:** 2409–2419.

Palmen, E. and C.W. Newton (1969), *Atmospheric circulation systems, International geophysics series, Academic Press, New York and London*, **13:** 471–560.

Pfeffer, R.L. and m. Challa (1981), A numerical study of the role of eddy fluxes of momentum in the development of Atlantic hurricanes, *J. Atmos. Sci.*, **38:** 2393–2398.

Rosinski, J. (1983), Mass and angular momentum diagnostics of hurricane Agnes during its transition to an extratropical cyclone, M.S. thesis, University of Wisconsin Madison, 67 pp.

Salmon, E.M. and P.J. Smith (1980), A synoptic analysis of the 25–26 January 1978 blizzard cyclone in the central United States, *Amer. Meteor. Soc.*, **2:** 70–83.

Strikwerda, J. C. (1989), Finite difference schemes and partial differential equaiton, Wadsworth and Brooks / cole, California, 386 pp.

Schubert, W.H. and B.T. Alworth (1987), Evolution of potential vorticity in tropical cyclones, *Q.J.R. Meteorol. Soc.*, **113:** 147–162.

Sundqvist, H. (1970), Numerical simulation of the development of tropical cyclones with a ten-level model, Part I, *Tellus*, **4:** 359–390.

Sutcliffe, R.C. (1947), A contribution to the problem of development, *Quart. J. Met. Soc.*, **73:** 370–383.

Wagner, A.J. (1978), Weather and circulation of January 1978–cold with record snowfall in the midwest and northeast, mild and wet in the west, *Mon. Wea. Rev.*, **106:** 579–585.

Wash, C.H. (1978), Diagnostics of observed and numerically simulated extratropical cyclones, Ph.D. thesis, University of Wisconsin–Madison, 215 pp.

Yuan, Z. (1990), On the forcing of the meridional circulation within cyclones: An isentropic study, M.S. thesis, University of Wisconsin Madison, 72 pp.

Yuan, Z. (1994), The role of the diabatic heating, torques and stability in forcing the meridional circulation within cyclones, Ph. D. thesis, University of Wisconsin Madison, 198 pp.